The role of potential vorticity anomalies in the Somali Jet on Indian summer monsoon intraseasonal variability

Article

Accepted Version

www.reading.ac.uk/centaur

1 **The role of potential vorticity anomalies in the Somali Jet on Indian Summer Monsoon**

2 **Intraseasonal Variability**

3 P. Rai[@], M. Joshi[#†], A. P. Dimri[@,*] and A. G. Turner[$]

4 [@]School of Environmental Sciences, Jawaharlal Nehru University, New Delhi, India

5 [#]Centre for Ocean and Atmospheric Sciences, University of East Anglia, Norwich, UK

6 [†]Climatic Research Unit, University of East Anglia, Norwich, UK

7 [$] NCAS-Climate and Department of Meteorology, University of Reading, Reading, UK

8 [*]For Correspondence: Prof. A. P. Dimri, School of Environmental Sciences, Jawaharlal Nehru

9 University, New Delhi, India, 110067. Email: apdimri@hotmail.com

10

11

12

13

14

15

16

17

18

19

20

21

22

23

24   **Abstract**

25   The climate of the Indian subcontinent is dominated by rainfall arising from the Indian summer

26   monsoon (ISM) during June to September. Intraseasonal variability during the monsoon is

27   characterized by periods of heavy rainfall interspersed by drier periods, known as active and

28   break events respectively. Understanding and predicting such events is of vital importance for

29   forecasting human impacts such as water resources. The Somali Jet is a key regional feature of

30   the monsoon circulation. In the present study, we find that the spatial structure of Somali Jet

31   potential vorticity (PV) anomalies varies considerably during active and break periods. Analysis

32   of these anomalies shows a mechanism whereby sea surface temperature (SST) anomalies

33   propagate north/northwestwards through the Arabian Sea, caused by a positive feedback loop

34   joining anomalies in SST, convection, modification of PV by diabatic heating and mixing in the

35   atmospheric boundary layer, wind-stress curl, and ocean upwelling processes. The feedback

36   mechanism is consistent with observed variability in the coupled ocean-atmosphere system on

37   timescales of approximately 20 days. This research suggests that better understanding and

38   prediction of monsoon intraseasonal variability in the South Asian monsoon may be gained by

39   analysis of the day-to-day dynamical evolution of PV in the Somali Jet.

40   **Keywords:** Indian Summer Monsoon (ISM), Somali Jet, Potential vorticity, Wind-stress curl,

41   Intraseasonal variability

42

1. Introduction

The summer monsoon during June to September (JJAS) is the chief contributor to total annual rainfall over the Indian subcontinent, through major rain-yielding systems such as monsoon depressions, the monsoon trough, offshore vortices, mid-tropospheric cyclones, as well as orographic rainfall over the Western Ghats. Rainfall is strongest during July and August (JA hereafter). Since Indian society is so finely tuned to the timing and intensity of the monsoon, any variations on time scales ranging from the intraseasonal to the interdecadal have huge impacts on a range of socio-economic sectors, mainly in agriculture, health and industry. The study of monsoon intraseasonal variability with its characteristic active and break periods of enhanced and reduced rainfall, each lasting several days or a week or more, is therefore of great importance for the Indian subcontinent.

Widespread research efforts (Rodwell, 1997; Krishnan et al., 2000; Krishnamurthy and Shukla, 2000, 2007, 2008; Gadgil and Joseph, 2003; Rajeevan et al., 2006, 2010; Maharana and Dimri, 2015) have shown how intra-seasonal variability (ISV) is expressed as active and break spells over the central Indian region during the monsoon (Goswami, 2005). Intraseasonal oscillations (ISOs) operating on time scales of around 30-60 days are accountable for much of the active and break events, in addition to the more widely recognized role played by external forcing such as the El Niño Southern Oscillation (ENSO), which adds a seasonal mean anomaly covering much of the country (Krishnamurthy and Shukla, 2000). The total amount of monsoon rainfall can be influenced by the length and relative frequency of active and break spells, which is primarily determined by the ISOs and their spatiotemporal evolution (Goswami, 2005; Sperber et al., 2000).

Forcing from sea-surface temperatures (SST) plays a very important role in monsoon variability, through e.g. ocean mixing in the Arabian Sea lowering SSTs and reducing convection and rainfall (Shenoi et al., 2002). Izumo et al. (2008) found variability in rainfall in western India was related to SST via variations in moisture transport associated with reduced upwelling off the Oman and Somali coasts. Further south, higher SSTs in the Seychelles-Chagos thermocline ridge region south of the equator cause reductions in upwelling, which are related to anomalously weak south–westerlies in late spring. Vecchi and Harrison (2004) showed a similar relationship between colder SST anomalies in the western Arabian Sea and decreased rainfall along the Western Ghats in June and July. In the Bay of Bengal, observations from BOBMEX observations have shown lowered SST during active phases of convection (Bhat, 2001).

On intraseasonal scales, observations from moored buoys suggest that SST varies primarily in response to variations in convection, decreasing in active spells and increasing in cloud free conditions (Premkumar et al., 2000). More detailed analysis reveals a quadrature relationship between Bay of Bengal SST and convection (with SST anomalies peaking 10-15 days before convective anomalies; Vialard et al., 2011; Jayakumar et al., 2016). The interaction of ocean with atmosphere during active and break cycle has been studied by Joseph and Sabin (2008). They observed the maximum positive SST anomaly value over north BoB prior to the beginning of an active-break cycle. At this time, the positive SST anomaly zone extends from the Arabian Sea to about longitude 150°E in the west Pacific Ocean which gives the mean SST anomaly of 11 active-break cycles in the 8 pentads (of an average active-break cycle of period 40 days). In the SST gradient area to the south of maximum SST anomaly, a convective cloud band forms after about a pentad that in the following 2–3 days generates an LLJ through peninsular India and the active phase of the monsoon begins. The cloud band thus formed

4

88 (reducing the incident solar radiation) and the strong winds of the LLJ (by causing evaporation

89 at the ocean surface) cools the ocean there, when the convection weakens and the LLJ moves

90 south to an equatorial location in the Indian Ocean which has warmer SST, where a new cloud

91 band forms. This is the break monsoon phase.

92 The studies by Findlater (1969, 1977) and Hart et al. (1978) define the East African Jet (EAJ)

93 and Somali Jet systems (henceforth we will describe these together as the Somali Jet) as the

94 critical elements of the low-level flow that supply the necessary moisture for supporting Indian

95 monsoon rains (Murakami et al., 1984), and are part of a circulation system that is set up by the

96 large-scale meridional tropospheric temperature gradient (Xavier et al., 2007). Any changes in

97 the temperature gradient can thus change the circulation pattern, leading to variations in seasonal

98 rainfall and timing of monsoon onset (Findlater, 1969). For instance, using monthly mean winds

99 Findlater (1971) showed that the LLJ splits into two branches over the Arabian Sea, the northern

100 branch intersecting the west coast of Indian near 17°N, while the southerly branch passes

101 eastward just south of India.

102 Krishnamurti et al. (1976) simulated the Somali Jet and its interaction with features such as the

103 orography over East Africa and Madagascar, using an imposed lateral forcing at 75°E to

104 represent the meridional land–ocean contrast in heating, essentially following Murakami et al.

105 (1970). Krishnamurti et al. (1976) concluded that the broad-scale Somali Jet was forced by the

106 land-ocean contrast in heating in this region, and barotropic instability was ascribed as a possible

107 mechanism for the splitting the Jet over the Arabian Sea. A study by Krishnan et al. (2000)

108 suggested that forcing by suppressed convection anomalies over the Bay of Bengal leads to the

109 development of low-level anticyclonic circulation anomalies as a Rossby wave response, which

110 then propagate northwestward to initiate the monsoon break over India.

111 Potential vorticity (PV) is an important quantity in the low-level monsoon circulation as

112 identified by Yang and Krishnamurti (1981); they assigned negative PV found in the Arabian

113 Sea north of the equator to advection from the southern hemisphere associated with the large-

114 scale monsoon circulation. Hoskins and Rodwell (1995) and Rodwell and Hoskins (1995)

115 studied the Somali Jet using a time-dependent primitive equation model with specified zonal

116 flow, mountains and diabatic heating, and showed how symmetric instabilities might be induced

117 by the transport of negative potential vorticity from the southern hemisphere into the atmosphere

118 overlying the Arabian Sea. Their study and others (e.g. Slingo et al., 2005) noted the importance

119 of the East African Highlands in confining the cross-equatorial flow into a zonally narrow jet.

120 Rodwell and Hoskins (1995) suggested that frictional and diabatic heating provided the

121 mechanism for material modification of PV within the Somali Jet and were essential in

122 sustaining it. They noted the strong sensitivity of the Somali Jet to changes in convective heating

123 over the southern Indian Ocean and that small modifications to PV led to anticyclonic circulation

124 of the Somali Jet over the Arabian Sea with a tendency of the flow to turn southeastward and

125 avoid India. According to them, the particles that retain their negative PV over the Arabian Sea

126 tend to recirculate back into the southern hemisphere, reducing moisture fluxes into the Indian

127 subcontinent.

128 A number of studies have appeared related to the variability in Somali Jet at interannual and

129 intraseasonal time scales (Webster et al., 1998; Annamalai et al., 1999; Sperber et al., 2000;

130 Krishnamurthy and Shukla, 2000; Goswami and Ajaya Mohan, 2001). However, little previous

131 research has examined the structure of PV anomalies in the Somali Jet and their relation to

132 monsoon rainfall over India. In our study, we focus on assessing the relationships between PV

133 anomalies in the Somali Jet near the equator and rainfall during active and break phases of the

134 Indian monsoon during the July and August season.

135 The remainder of this paper is organized as follows. Section 2 contains details of the datasets

136 used and methodology followed. Section 3 discusses results of our analysis of the monsoon

137 dynamics during active and break phases, along with evolution of Somali Jet PV during these

138 phases. Conclusions are presented in Section 4.

139 **2. Data and Methodology**

140 We use the daily 0.5° resolution rainfall gridded dataset developed by the Indian Meteorological

141 Department (IMD) for the months of July and August. The reason for not including June and

142 September in the present study is because during those months, ISM signals are likely to be

143 contaminated by the onset and withdrawal phases of the monsoon, respectively. The dataset is

144 well validated and reliable (Rajeevan and Bhate, 2008) and available from 1971 to 2005 with a

145 domain starting at 6.5°N, 66.5°E (as the south-west corner) over a total of 69x65 grid points. As

146 a proxy for large-scale convection of tropical regions we use the interpolated Outgoing

147 Longwave Radiation (OLR) data of Liebmann and Smith (1996) obtained from

148 NOAA/OAR/ESRL PSD, Boulder, Colorado from http://www.esrl.noaa.gov/psd on a 2.5°x

149 2.5°global grid.

150 Global atmospheric and surface fields are extracted from the European Centre for Medium

151 Range Weather Forecasts (ECMWF) Interim Re-Analysis data (Dee et al., 2011; ERA-Interim

152 hereafter) from 1979 to 2005. ERA-Interim operates at a spectral T255 horizontal resolution

153 corresponding to approximately 79 km spacing on a reduced Gaussian grid at 6-hourly time

154 means and on 60 vertical levels, with the model top at 0.1 hPa (about 64 km). Data used in the

155 atmosphere are: PV at 850 hPa, zonal and meridional wind components (u and v), air

7

156 temperature (T), vertical velocity (ω), specific humidity (q) and geopotential height (z) at the

157 1000-, 925-, 850-, 700-, 600, 500-, 400-, and 300-hPa pressure levels. The study period chosen is

158 based on the availability of corresponding IMD rainfall observations at $0.5° \times 0.5°$ resolution,

159 which is limited to the period 1979-2005 (Rajeevan and Bhate, 2008). Climatological means and

160 anomalies are estimated for each of the selected variables from the reanalysis data for the peak

161 monsoon season (JA) and the anomalies plotted for all the selected variables are relative to the

162 climatology for July-August for the period 1979-2005.

163 To understand the dynamics of the Somali Jet, PV anomalies and associated variables at 850 hPa

164 have been plotted over the region 0°N-25°N, 45°E-80°E, shown in Fig. 1 (Box-1) during active

165 and break spells of the monsoon. Based on the spatial structure of Somali Jet PV anomalies over

166 Box-1, this region has been selected for further discussion of Somali Jet PV dynamics because it

167 is representative of PV transport and associated convection.

168 The potential vorticity equation as mentioned in Rodwell and Hoskins (1995) can be written as:

169 $\frac{DP}{Dt} = \frac{1}{\rho} F_\zeta . \nabla\theta + \frac{1}{\rho} \zeta . \nabla\dot\theta$,

170 where P is potential vorticity, ∇ is 3D gradient operator, $F_\zeta = \nabla \times F_v$, (the 3D curl of

171 momentum forcing) and $\dot\theta = D\theta/Dt$. The two terms on the right-hand side of the PV equation

172 represent the material modification to PV due to frictional and diabatic effects respectively.

173 **2.1 Defining active and break phases**

174 To obtain the dates of active and break events we use an index over the Monsoon Core Region

175 (hereafter MCR; 73°E-82°E and 18°-28°N as in Mandke et al., 2007). For preparing the daily

176 rainfall time series from IMD data over MCR, area averaging has been performed for JA over

177 the period 1979-2005. For the calculation of the daily-standardized anomaly rainfall time series,

178 the daily precipitation anomaly to the climatological seasonal cycle is divided by the daily-

179   evolving standard deviation of the time series. Based on this standardized anomaly time series,

180   active (break) spells are distinguished as periods when the value of the standardized anomaly for

181   the rainfall is greater than +1 (less than −1) standard deviation for at least three consecutive days.

182   The corresponding dates (as listed in Table 1) are then used to select corresponding active and

183   break phases from ERA-Interim and other datasets over the 1979-2005 period. The method used

184   is similar to that in Rajeevan et al. (2006). Some of the active and break spell dates of this study

185   during JA do not coincide with observations in some previous studies in some of the years but

186   they compare well to the dates given by Maharana and Dimri (2015). This slight mismatch in the

187   dates can be attributed to length of study period chosen: since rainfall is considered over the

188   MCR for JA only, some events are missed at the June-July and July-August boundaries.

189   **2.2 Diabatic heating**

190   The thermodynamic energy equation presented in Newell et al. (1974), in pressure coordinates, is

191   used for the calculation of the diabatic heating term:

192
$$\frac{\partial \overline{T}}{\partial t} + \frac{1}{a}\left(\frac{\overline{u}}{cos\phi}\frac{\partial \overline{T}}{\partial \lambda} + \overline{v}\frac{\partial \overline{T}}{\partial \phi}\right) + \overline{\omega}\left(\frac{\partial \overline{T}}{\partial p} - \frac{R\overline{T}}{c_p p}\right) = \overline{\dot{Q}}$$

193   where cp is the specific heat of dry air at levels of constant pressure, R is the gas constant for dry

194   air, and p is the pressure. The heating term $\dot{Q}$ includes contributions by the transfer of heat by

195   turbulent and molecular conduction $\dot{Q}$s, from latent heat release $\dot{Q}_l$, and by radiative processes

196   $\dot{Q}$r. Diabatic heating rate fields are computed from the above equation as a residual, using daily

197   data from ERA-Interim. The quantities with bars above indicate time averages.

198   **3. Results**

199   Lagged composites of different meteorological parameters have been studied here in order to

200   understand how different processes and signals change and propagate during mean active and

201   break phases. These composites have been generated using the standardized rainfall anomaly in

202   the MCR region as described in Section 2.1, with lags over the range ±10 days. A composite of

203   original dates of active and break spells calculated for JA months from the period 1979-2005 is

204   chosen as lag00. Other lag dates are calculated with respect to the peak day (for example, if the

205   peak (lag=0) date is 20th July, then the lag+02 date is 22nd July, etc.).

206   Lagged composites of daily rainfall anomalies over the whole Indian landmass are shown in Fig.

207   2a and b for active and break phases respectively. Fig. 2a shows the movement of a band of

208   positive rainfall anomalies from southern India to the monsoon core zone, i.e. generally

209   northwards, over the development of the active event, i.e. from lag-10 to lag00. Shortly after the

210   peak, negative rainfall anomalies exist over the foothills of the Himalayas and the southeast

211   peninsula region, the latter being a rain shadow region, receiving reduced rainfall in the lee of the

212   Western Ghats mountains. The period from lag-02 to lag+02 also shows the propagation of very

213   large positive rainfall anomalies from the east coast adjoining the Bay of Bengal (BoB) towards

214   the northwest, suggestive of moving anomalies up the monsoon trough. The lagged composites

215   during the break phase (Fig. 2b) show a general reversal of the rainfall anomalies compared to

216   active phases, with negative rainfall anomalies over the Western Ghats, and general northward

217   propagation of negative anomalies from the western part of central India at lag-08, covering the

218   whole central region by lag-04 and with more intense anomalies by lag00. The evolution of

219   rainfall during active and break phases of the monsoon is discussed in more detail by

220   Krishnamurthy and Shukla (2000, 2007, 2008), Rajeevan and Bhate (2008) and Maharana and

221   Dimri (2016).

222   Rainfall over India is supported largely via the transport of moisture from the Arabian Sea and

223   southern Indian Ocean by the strong cross-equatorial Somali Jet winds (Findlater, 1969; Naidu et

224   al., 2011a). On interannual and intraseasonal timescales, variations in SST in the tropical Indian

225 Ocean are also known to be strongly affected by monsoon wind variability (McCreary et al.,

226 1993; Sengupta et al., 2001; Ramesh and Krishnan, 2005). Lagged composites of wind

227 anomalies at 850 hPa during active and break periods are presented in Fig. 3a, b respectively.

228 The lagged composite of wind-speed anomalies during active spells (Fig. 3a) shows a negative

229 anomaly over northern India that moves northwards as time continues towards lag00.

230 Conversely, during break periods (Fig. 3b), exactly the opposite pattern is observed, i.e. weaker

231 westerlies during lag-04 to lag+02 and negative wind anomalies over the MCR region and

232 Arabian Sea.

233 The PV budget calculation by Rodwell and Hoskins (1995) demonstrated how the change in sign

234 in Coriolis parameter at the equator prevents cross-equatorial flow in the absence of material

235 tendencies in PV. They showed that the frictional torque exerted by the East African Highlands

236 on the Somali Jet is an important mechanism for modifying PV. According to Rodwell and

237 Hoskins (1995), when there is very little further modification of the PV, the Somali Jet turns

238 anticyclonically over the Arabian Sea and the flow tends to avoid India. Lagged composites of

239 PV during active and break periods (figure not shown) over the Arabian Sea at 850 hPa have

240 been plotted in order to show the spatial pattern of PV advection during these periods which

241 display advection of negative PV across the equator into the Northern Hemisphere over the

242 western Indian Ocean. While there are many similarities between active and break phases, the

243 periods immediately before the peak active phase, and 6 days after the peak break, do display

244 more negative PV anomalies upstream over the western equatorial Indian Ocean.

245 The PV anomalies themselves are shown in Figs. 4a and 4b for active and break periods

246 respectively. The regions in Figs 4a and 4b have been selected in order to get an overview of PV

247 behavior over the whole Arabian Sea rather than just over the SW region. During active spells, a

248 negative PV anomaly exists in the south-eastern quadrant of the Arabian Sea, consistent with a

249 lack of material modification of PV, which is then manifested by a stronger Somali Jet that

250 curves to the east over southern India (See Fig. 3a). This negative PV anomaly weakens after

251 lag00. During break periods (Fig. 4b), the opposite pattern exists: positive PV anomalies in the

252 south eastern region of the Arabian Sea imply greater modification of PV by diabatic

253 mechanisms, and weaker westerly winds over southern India (see Fig. 3b); the positive PV

254 anomaly gets stronger from lag-10 to lag00, before becoming weaker as time moves past the

255 peak of the break period.

256 In order to examine the vertical structure of the PV anomalies, they are shown at the 500 hPa

257 level in Fig. 5a and 5b. During active periods (Fig. 5a), negative PV anomalies mostly cover the

258 central and western Arabian Sea at lag00, before dissipating in time by lag+10. During break

259 periods (Fig. 5b), the converse is true: modified, i.e. positive, PV anomalies occur over the

260 Arabian Sea region which again dissipate by lag +10.

261 The concept of PV has been found particularly helpful by Hoskins et al (1985) to analyze the

262 role of diabatic processes in the development of PV anomalies. In order to explain the material

263 modification in Somali Jet PV, we have examined daily diabatic heating anomalies at 850 hPa

264 for lag-10 to +10 in active and break periods; the results are shown in Fig. 6a and 6b

265 respectively. During active periods (Fig. 6a), negative diabatic heating anomalies build over the

266 southern Arabian Sea, indicating less convection (and hence less PV modification) from lag-06

267 to lag+06. During break events (Fig. 6b), there is an east-west split in the southern Arabian Sea,

268 with the eastern half covered by negative diabatic heating anomalies between lag-10 to lag00,

269 which dissipate by lag +10.

270   The large-scale pattern of convection has been shown in order to understand the thermodynamic

271   state of atmosphere and its variability during the modification of PV that prevails in different

272   phases of monsoonal season using outgoing longwave radiation (OLR, contour) and lagged

273   composites of SST (shaded) anomalies for active and break spells is shown in Fig. 7a and b

274   respectively between lag-10 to +10. During an active spell (Fig. 7a, contour) a strong negative

275   OLR anomaly covers most of the Arabian Sea region and Western Ghats, consistent with

276   enhanced deep cloud cover, while a positive anomaly can be seen south of the Indian peninsula,

277   which slowly moves northwards as time progresses. Between lag+02 and lag+10, positive

278   anomalies grow over most of the Arabian Sea region especially between lag+08 and lag+10. The

279   NW-SE split in OLR anomalies mirrors the shape of PV anomalies, such that in the SE quadrant

280   of the Arabian Sea, positive OLR anomalies developing following an active phase imply reduced

281   convection, less mixing in the atmospheric BL, a shoaling of the atmospheric BL, and less

282   material modification of PV; this results in the negative PV anomalies displayed in the positive

283   lags of Fig. 4a, and the anticyclonic curvature of winds over the south of India. Since break

284   phases develop following the transition from active periods, breaks (Fig. 7b, contour) are

285   characterized by the presence of strong positive OLR anomalies that completely cover the

286   Somali Jet PV region from lag-08 to lag-02, but then move northwards as time progresses. The

287   break periods suggest more modification of PV by convection and boundary layer mixing, and a

288   deeper mixing in the atmospheric BL leading to deepening of the atmospheric BL over the

289   northern Arabian Sea, which is consistent with winds curving weakly i.e. weaker south

290   westerlies over the northern half of India (See Fig. 3b).

291   For SST anomalies, during active periods, the NW/SE split is again apparent, with a band of

292   anomalously cold SSTs that moves slowly northwestwards from lag-10 to+10, removing the

293 warm SST anomaly in the northern Arabian Sea during lags-10 to lag-04. The presence of colder

294 SSTs is because of enhanced upwelling of relatively cold subsurface oceanic water by windstress

295 curl anomalies (see later). The cold anomalies appear to slightly lead the similar northwestward

296 movement of warm OLR anomalies (See Fig. 7a, shaded), which is consistent with colder SSTs

297 inhibiting convection and increasing OLR. During the break periods (Fig. 7b, shaded), weaker

298 winds cause less upwelling, and warm SST anomalies slowly move northwards across the

299 Arabian Sea from lag-06 to lag+06. The north-south dipole seen during both active and break

300 periods is hereafter referred as the Arabian Sea Dipole (ASD), and is similar to other dipoles

301 observed both in the Arabian Sea and the Bay of Bengal during active and break phases

302 (Krishnan et al., 2000).

303 The spatial structure of wind stress is important in understanding how wind forcing affects ocean

304 upwelling, and the consequent effects on SST. Lagged composites of anomalies of wind stress

305 and their curl are plotted in Fig. 8. The anomalies display a similar pattern to the winds shown in

306 Fig. 3. During active phases, strong positive wind stress curl anomalies force oceanic upwelling

307 and cooling on the northern/northwestern flank of the Somali Jet up to lag+02, while a negative

308 windstress curl pattern builds on the southern/southeastern flank of the Somali Jet from lags-06

309 to+02, which tends to reduce upwelling and raise SST. These patterns are consistent with the

310 cold SST anomalies displayed in Fig. 7a (shaded) that are slowly shunted northwestwards.

311 During break periods (Fig. 8b), a similar but opposite pattern of wind stress curl and wind stress

312 is observed; positive wind stress curl on the southern/southeastern flank from lag-04 to lag+04,

313 and negative wind stress curl on the northern/northwestern flank. These patterns of wind stress

314 curl and wind stress during active and break periods are in agreement with the results of

315 Anderson et al. (1992).

316 As an example, the lagged correlations between PV versus SST and PV versus rainfall are shown

317 in Fig. 9. The correlation between PV and SST shows a high positive correlation at lag-04 which

318 indicates the lagging of PV by SST on a scale of 4 days while a maximum negative correlation

319 between PV and rainfall can be seen at lag00.

320 **4. Discussion and Conclusions**

321 The above results suggest a potential feedback loop that connects various aspects of

322 intraseasonal monsoon core region (MCR) rainfall and offer a mechanism for the propagation of

323 related anomalies. Key to the feedback is the northwest/southeast split in PV anomaly and

324 windstress curl in the Arabian Sea. A schematic of such a feedback for active and break phases is

325 shown in Fig. 10, and described here.

326 If one considers an active period anomaly over the south eastern Arabian Sea, an oceanic Rossby

327 wave for instance might cause a negative SST anomaly (Fig. 7a, shaded) lag-08 to -04). The

328 Somali Jet in this region has a negative PV anomaly in its southern flank and a positive PV

329 anomaly on its northern flank (Fig. 4a lag-08 to 00). This negative SST anomaly will be

330 associated with reduced evaporation, less convection and higher OLR (Fig. 7a, contour) lag-08 to

331 -04), which leads to less mixing of PV. The negative PV anomaly acts to curve the flow

332 anticyclonically, causing a negative (downwelling) windstress curl anomaly on the jet's southern

333 flank (Fig. 8a lag-06 to +02), and thus surface warming there. Conversely the positive PV

334 anomaly on the jet's northern flank acts to curve the flow cyclonically, causing an upwelling

335 windstress curl, and a surface cooling north of the jet. Because the mixed layer is deeper towards

336 the south of the jet, the overall effect is to cool the northern Arabian Sea more quickly than the

337 southern Arabian Sea warms (Fig. 7a, shaded) lag00 to +10).

15

338   On the other hand, if one considers a break period anomaly, a positive SST anomaly (Fig 7b,

339   shaded) lag-08 to -04) leads to more evaporation, more convection and lower OLR over the

340   southern Arabian Sea (Fig. 7b, contours) lag-04 to +02), which leads to more mixing of PV: The

341   Somali Jet in this region then has a positive PV anomaly on its southern flank and a negative PV

342   anomaly on its northern flank (Fig. 4b lag-04 to +02). The positive PV anomaly acts to curve the

343   flow cyclonically, causing a positive (upwelling) windstress curl anomaly on the jet's southern

344   flank (Fig. 8b lag-04 to +04), and surface cooling south of the Jet. Again, because the mixed

345   layer is deeper towards the south of the jet, the overall effect is to warm the northern Arabian Sea

346   faster than the southern Arabian Sea cools (Fig. 7b, shaded) lag00 to +10).

347   The descriptions above deal with the onset of the anomalous winds, but not the timescale over

348   which the wind anomalies decay: this happens after lag+02 for active events, and after lag+06

349   for break events. For active events, the slow warming developing over the southern Arabian Sea

350   (Fig. 7a, shaded) lag+02 to +10) allows more evaporation, convection, mixing and PV

351   modification, reducing the negative PV anomaly (Fig 4a lag+04 to +10); the opposite (cooling

352   and reduction of positive PV anomalies) happens following break events. Additionally, during

353   active events, high vertical wind shear in the BL might itself cause large amounts of mixing and

354   PV modification. Consideration of PV anomalies therefore allows a mechanism whereby SST

355   anomalies build and propagate northwestwards through the Arabian Sea during active and break

356   periods.

357   The timescale for the feedback is essentially set by the timescales for anomalies in diabatic

358   forcing to change Somali Jet PV, and for resulting wind stress curl anomalies to force vertical

359   ocean velocities in the mixed layer that significantly change SST. It can be estimated in a similar

360   manner to Marshall et al. (2001) and O'Callaghan et al. (2014) by expressing the Ekman-induced

361   transport as a pseudo heat flux $H_E = c_p \Delta SST \, \nabla \times \tau \,/ f$, where ΔSST is the horizontal SST

362   gradient across the domain (or ~2 K), c_p is the specific heat capacity of water, $\nabla \times \tau$ is estimated

363   from Fig. 8, and $f \approx 2 \times 10^{-5} \mathrm{s}^{-1}$. The temperature change of the surface can then be calculated

364   assuming that the heat flux is distributed throughout the mixed layer, which we assume is 40 m

365   deep. Following the peak of an active event, $H_E \approx 20 \, \mathrm{Wm}^{-2}$, implying a change in

366   temperature of O(0.1) K (the size of the anomalies that emerge in the south eastern corner of the

367   panels in Fig. 7 (shaded)) over 10 days.

368   While the precise role of PV anomalies in the Somali Jet on the intensity and structure of

369   different phases of ISM rainfall is debated, it has been broadly acknowledged in previous studies

370   that modification in PV is required in order to avoid breaks in the monsoon (Rodwell and

371   Hoskins, 1995; Rodwell, 1997; Joseph and Sijikumar, 2004). Our work suggests a more complex

372   picture of PV whereby during an active event, PV modification (from negative to positive) is

373   minimal over the Arabian Sea, but mainly happens as the flow crosses the peninsula and turns

374   cyclonically northward, causing a low pressure anomaly. Conversely, during a break, PV is

375   being significantly modified upstream over the Arabian Sea, weakening the jet and reducing flow

376   onto the Indian peninsula: the result is an absence of convergence over India, and a lack of

377   rainfall.

378   Simulating ISM variability therefore requires coupled ocean-atmosphere GCMs that represent

379   the above feedbacks correctly, such as the oceanic mixed layer response to a wind stress curl

380   anomaly, and convection and subsequent PV modification response to an SST anomaly. If

381   feedbacks such as these are weak in GCMs, then ISM variability may be too weak; conversely, if

382   such feedbacks are too strong, ISM variability may be so strong that mean rainfall can be

383   significantly biased. We therefore speculate that adequate vertical resolution of the upper ocean

17

384 is necessary in order to resolve PV-driven interactions with the oceanic mixed layer. In addition,

385 since key elements of these feedbacks such as ocean mixed layer processes and convection are

386 parametrized, we suggest that analysis of such feedbacks in a variety of coupled ocean-

387 atmosphere GCMs should be performed in future.

388 Climate model projections of the ISM later in this century suggest increased mean rainfall, but

389 greater variability (e.g. as reviewed in Turner and Annamalai, 2012). Warmer SSTs suggest

390 shallower ocean mixed layers (though the dynamical influence of ISM winds on the ocean is

391 important over the Arabian Sea), and potentially a different relationship between convection and

392 the response of PV modification to an SST anomaly, e.g. due to changed humidity and lapse

393 rates. Analysis of how GCMs simulate present-day PV behavior in different phases of the ISM

394 may therefore shed light on understanding ISM variability in different GCM projections of 21st

395 century climate change.

396 In the present study, we have examined the variability of rainfall on intraseasonal time scales and

397 atmospheric processes associated with it over the monsoon core region (MCR; as a

398 representative region of Indian monsoon variability) and its relation with PV anomalies in the

399 Somali Jet during different phases of the ISM. By shedding light on the response of the ISM to

400 modified PV, and resulting flow – precipitation interactions, this study will contribute to better

401 understanding the influence of Somali Jet dynamics on the monsoon on different time scales.

References

Anderson, D. M., and Prell, W. L. (1992). The structure of the southwest monsoon winds over the Arabian Sea during the late Quaternary: Observations, simulations, and marine geologic evidence. *Journal of Geophysical Research: Oceans*, *97*(C10), 15481-15487.

Anderson, D. M., Brock, J. C., and Prell, W. L. (1992). Physical upwelling processes, upper ocean environment and the sediment record of the southwest monsoon. *Geological Society, London, Special Publications*, *64*(1), 121-129.

Annamalai, H., Slingo, J. M., Sperber, K. R., and Hodges, K. (1999). The mean evolution and variability of the Asian summer monsoon: Comparison of ECMWF and NCEP-NCAR reanalyses. *Monthly Weather Review*, *127*(6), 1157-1186.

Bhat G.S. (2001). Near surface atmospheric characteristics over the North Bay of Bengal during the Indian Summer Monsoon. *Geophysical Research Letters,* 28:987–90.

Dee, D. P., Uppala, S. M., Simmons, A. J., Berrisford, P., Poli, P., Kobayashi, S., ... and Bechtold, P. (2011). The ERA-Interim reanalysis: Configuration and performance of the data assimilation system. *Quarterly Journal of the royal meteorological society*, *137*(656), 553-597.

Findlater, J. (1969). A major low-level air current near the Indian Ocean during the northern summer. *Quarterly Journal of the Royal Meteorological Society*, *95*(404), 362-380.

Findlater, J. (1971). *Mean monthly airflow at low levels over the western Indian Ocean* (No. 116). HM Stationery Office.

Findlater, J. (1977). Observational aspects of the low-level cross-equatorial jet stream of the western Indian Ocean. *Pure and Applied Geophysics*,*115*(5-6), 1251-1262.

Goswami BN. (2005). South Asian monsoon. In *Intraseasonal Variability in the Atmosphere-Ocean Climate System*, ed. WKM Lau, DE Waliser, pp. 19–61. Berlin: Praxis Springer.

Goswami, B. N., Ajayamohan, R. S., Xavier, P. K., and Sengupta, D. (2003). Clustering of

431 synoptic activity by Indian summer monsoon intraseasonal oscillations. *Geophysical Research*

432 *Letters*, *30*(8).

433 Goswami, B. N., and Ajayamohan, R. S. (2001). Intraseasonal oscillations and interannual

434 variability of the Indian summer monsoon. *Journal of Climate*, 14, 1180-1198.

435 Hart, J. E., Rao, G. V., Van De Boogaard, H., Young, J. A., and Findlater, J. (1978). Aerial

436 observations of the East African low-level jet stream. *Monthly Weather Review*, *106*(12), 1714-

437 1724.

438 Hoskins, B. J., McIntyre, M. E., and Robertson, A. W. (1985). On the use and significance of

439 isentropic potential vorticity maps. *Quarterly Journal of the Royal Meteorological*

440 *Society*, *111*(470), 877-946.

441 Hoskins, B. J., and Rodwell, M. J. (1995). A model of the Asian summer monsoon. Part I: The

442 global scale. *Journal of the Atmospheric Sciences*, *52*(9), 1329-1340.

443 Huang, N. E., Shen, Z., Long, S. R., Wu, M. C., Shih, H. H., Zheng, Q., ... and Liu, H. H. (1998,

444 March). The empirical mode decomposition and the Hilbert spectrum for nonlinear and non-

445 stationary time series analysis. In *Proceedings of the Royal Society of London A: Mathematical,*

446 *Physical and Engineering Sciences* (Vol. 454, No. 1971, pp. 903-995). The Royal Society.

447 Izumo, T., Montégut, C. B., Luo, J. J., Behera, S. K., Masson, S., and Yamagata, T. (2008). The

448 role of the western Arabian Sea upwelling in Indian monsoon rainfall variability. *Journal of*

449 *Climate*, *21*(21), 5603-5623.

450 Jayakumar, A., Turner, A. G., Johnson, S. J., Rajagopal, E. N., Mohandas, S. and Mitra, A. K.

451 (2016). Boreal summer sub-seasonal variability of the South Asian monsoon in the Met Office

452 GloSea5 initialized coupled model. *Climate Dynamics*, published online, doi:10.1007/s00382-

453 016-3423-x.

454 Joseph, P. V., and Sabin, T. P. (2008). An ocean–atmosphere interaction mechanism for the

455 active break cycle of the Asian summer monsoon. *Climate dynamics*, *30*(6), 553-566.

456 Joseph, P. V., and Sijikumar, S. (2004). Intraseasonal variability of the low-level jet stream of

457 the Asian summer monsoon. *Journal of Climate*, *17*(7), 1449-1458.

458 Joseph, P. V., Eischeid, J. K., and Pyle, R. J. (1994). Interannual variability of the onset of the

459 Indian summer monsoon and its association with atmospheric features, El Nino, and sea surface

460 temperature anomalies. *Journal of Climate*, *7*(1), 81-105.

461 Krishnamurthy, V., and Shukla, J. (2000). Intraseasonal and interannual variability of rainfall

462 over India. *Journal of Climate*, *13*(24), 4366-4377.

463 Krishnamurthy, V., and Shukla, J. (2007). Intraseasonal and seasonally persisting patterns of

464 Indian monsoon rainfall. *Journal of climate*, *20*(1), 3-20.

465 Krishnamurthy, V., and Shukla, J. (2008). Seasonal persistence and propagation of intraseasonal

466 patterns over the Indian monsoon region. *Climate Dynamics*, *30*(4), 353-369.

467 Krishnamurti, T. N., and Ramanathan, Y. (1982). Sensitivity of the monsoon onset to differential

468 heating. *Journal of the Atmospheric Sciences*, *39*(6), 1290-1306.

469 Krishnamurti, T. N., and Wong, V. (1979). A planetary boundary-layer model for the Somali

470 Jet. *Journal of the Atmospheric Sciences*, *36*(10), 1895-1907.

471 Krishnamurti, T. N., Molinari, J., and Pan, H. L. (1976). Numerical simulation of the Somali

472 jet. *Journal of the Atmospheric Sciences*, *33*(12), 2350-2362.

473 Krishnamurti, T. N., Wong, V., Pan, H. L., Pasch, R., Molinari, J., and Ardanuy, P. (1983). A

474 three-dimensional planetary boundary layer model for the Somali jet. *Journal of the Atmospheric*

475 *Sciences*, *40*(4), 894-908.

21

476 Krishnan, R., Zhang, C., and Sugi, M. (2000). Dynamics of breaks in the Indian summer

477 monsoon. *Journal of the Atmospheric Sciences*, *57*(9), 1354-1372.

478 Liebmann, B. (1996). Description of a complete (interpolated) outgoing longwave radiation

479 dataset. *Bulletin of the American Meteorological Society*, *77*, 1275-1277.

480 Maharana, P., and Dimri, A. P. (2016). Study of intraseasonal variability of Indian summer

481 monsoon using a regional climate model. *Climate Dynamics*,*46*(3-4), 1043-1064.

482 Mandke, S. K., Sahai, A. K., Shinde, M. A., Joseph, S., and Chattopadhyay, R. (2007).

483 Simulated changes in active/break spells during the Indian summer monsoon due to enhanced

484 CO2 concentrations: assessment from selected coupled atmosphere–ocean global climate

485 models. *International journal of climatology*, *27*(7), 837-859.

486 Marshall J., Johnson, H. and Goodman J. (2001). A Study of the Interaction of the North Atlantic

487 Oscillation with Ocean Circulation. *Journal of Climate*, 14, 1399-1421.

488 McCreary, J. P., Kundu, P. K., and Molinari, R. L. (1993). A numerical investigation of

489 dynamics, thermodynamics and mixed-layer processes in the Indian Ocean. *Progress in*

490 *Oceanography*, *31*(3), 181-244.

491 Murakami, T., R. Godbole, and R. R. Kelkar, 1970: Numerical simulation of the monsoon along

492 80°E. *Proc. Conf. on the Summer Monsoon of South East Asia,* Norfolk, VA, Navy Weather

493 Research Facility, 39–51.

494 Murakami, T., Nakazawa, T., and He, J. (1984). On the 40-50 day oscillations during the 1979

495 Northern Hemisphere summer. I: Phase propagation. *Journal of the Meteorological Society of*

496 *Japan*, *62*(3), 440-468.

497 Naidu, C. V., Krishna, K. M., Rao, S. R., Kumar, O. B., Durgalakshmi, K., and Ramakrishna, S.

498 S. V. S. (2011). Variations of Indian summer monsoon rainfall induce the weakening of easterly

499 jet stream in the warming environment? *Global and Planetary Change*, *75*(1), 21-30.

500 Newell, R. E., Kidson, J. W., Vincent, D. G., and Boer, G. J. (1974). General circulation of the

501 tropical atmosphere and interactions with extratropical latitudes. *Volume 2* (No. COO-2195-16).

502 Massachusetts Institute of Technology Press, Cambridge, MA.

503 O'Callaghan, A., Joshi, M., Stevens, D. and Mitchell, D. (2014). The effects of different sudden

504 stratospheric warming types on the ocean. *Geophysical Research Letters*, 41, DOI:

505 10.1002/2014GL062179.

506 Premkumar, K., Ravichandran, M., Kalsi, S. R., Sengupta, D., and Gadgil, S. (2000). First results

507 from a new observational system over the Indian seas. *Current Science*, *78*(3), 323-330.

508 Rajeevan, M., and Bhate, J. (2009). A high resolution daily gridded rainfall dataset (1971–2005)

509 for mesoscale meteorological studies. *Current Science*, *96*(4), 558-562.

510 Rajeevan, M., Bhate, J., Kale, J. D., and Lal, B. (2006). High resolution daily gridded rainfall

511 data for the Indian region: Analysis of break and active monsoon spells. *Current Science*, *91*(3),

512 296-306.

513 Rajeevan, M., Gadgil, S., and Bhate, J. (2010). Active and break spells of the Indian summer

514 monsoon. *Journal of earth system science*, *119*(3), 229-247.

515 Ramesh, K. V., and Krishnan, R. (2005). Coupling of mixed layer processes and thermocline

516 variations in the Arabian Sea. *Journal of Geophysical Research: Oceans*, *110*(C5).

517 Rodwell, M. J. (1997). Breaks in the Asian monsoon: The influence of Southern Hemisphere

518 weather systems. *Journal of the Atmospheric Sciences*, *54*(22), 2597-2611.

519   Rodwell, M. J., and Hoskins, B. J. (1995). A model of the Asian summer monsoon. Part II:

520   Cross-equatorial flow and PV behavior. *Journal of the Atmospheric Sciences*, *52*(9), 1341-1356.

521   Sengupta, D., and Ravichandran, M. (2001). Oscillations of Bay of Bengal sea surface

522   temperature during the 1998 summer monsoon. *Geophysical Research Letters*, *28*(10), 2033-

523   2036.

524   Shenoi, S. S. C., Shankar, D., and Shetye, S. R. (2002). Differences in heat budgets of the near-

525   surface Arabian Sea and Bay of Bengal: Implications for the summer monsoon. *Journal of*

526   *Geophysical Research: Oceans*, *107*(C6).

527   Shukla, J. (1987a). Interannual variability of monsoons, *Monsoons.* J. S. Fein, P. L.

528   Stephens, 399–464, John Wiley and Sons.

529   Shukla, J., and Misra, B. M. (1977). Relationships between sea surface temperature and wind

530   speed over the central Arabian Sea, and monsoon rainfall over India. *Monthly Weather*

531   *Review*, *105*(8), 998-1002.

532   Slingo, J., Spencer, H., Hoskins, B., Berrisford, P., and Black, E. (2005), The meteorology of the

533   Western Indian Ocean, and the influence of the east African highlands. *Philosophical*

534   *Transactions of the Royal Society of London A*, 363, 25–42.

535   Sperber, K. R., Slingo, J. M., and Annamalai, H. (2000). Predictability and the relationship

536   between subseasonal and interannual variability during the Asian summer monsoon. *Quarterly*

537   *Journal of the Royal Meteorological Society*,*126*(568), 2545-2574.

538   Turner, A. G. and Annamalai, H. (2012). Climate Change and the South Asian summer

539   monsoon. *Nature Climate Change*, 2, 587-595.

540   Vecchi, G. A., and Harrison, D. E. (2002). Monsoon Breaks and Subseasonal Sea Surface

541   Temperature Variability in the Bay of Bengal. *Journal of Climate*, *15*(12), 1485-1493.

542   Vialard, J., Jayakumar, A., Gnanaseelan, C., Lengaigne, M., Sengupta, D. and Goswami, B

543   (2011). Processes of 30–90 days' sea surface temperature variability in the northern Indian

544   Ocean during boreal summer. *Climate Dynamics*, 38(9–10): 1901–1916.

545   Webster, P. J., Magana, V. O., Palmer, T. N., Shukla, J., Tomas, R. A., Yanai, M. U., and

546   Yasunari, T. (1998). Monsoons: Processes, predictability, and the prospects for

547   prediction. *Journal of Geophysical Research: Oceans*, 103(C7), 14451-14510.

548   Wu, Z., and Huang, N. E. (2004). A study of the characteristics of white noise using the

549   empirical mode decomposition method. In *Proceedings of the Royal Society of London A:*

550   *Mathematical, Physical and Engineering Sciences* (Vol. 460, No. 2046, pp. 1597-1611). The

551   Royal Society.

552   Wu, Z., and Huang, N. E. (2009). Ensemble empirical mode decomposition: a noise-assisted data

553   analysis method. *Advances in adaptive data analysis*, *1*(01), 1-41.

554   Xavier, P. K., Marzin, C., and Goswami, B. N. (2007). An objective definition of the Indian

555   summer monsoon season and a new perspective on the ENSO–monsoon relationship. *Quarterly*

556   *Journal of the Royal Meteorological Society*, *133*(624), 749-764.

557   Yang, D. S., and Krishnamurti, T. N. (1981). Potential vorticity of monsoonal low-level

558   flows. *Journal of the Atmospheric Sciences*, *38*(12), 2676-2695.

559   Zhang, J., Yan, R., Gao, R. X., and Feng, Z. (2010). Performance enhancement of ensemble

560   empirical mode decomposition. *Mechanical Systems and Signal Processing*, *24*(7), 2104-2123.
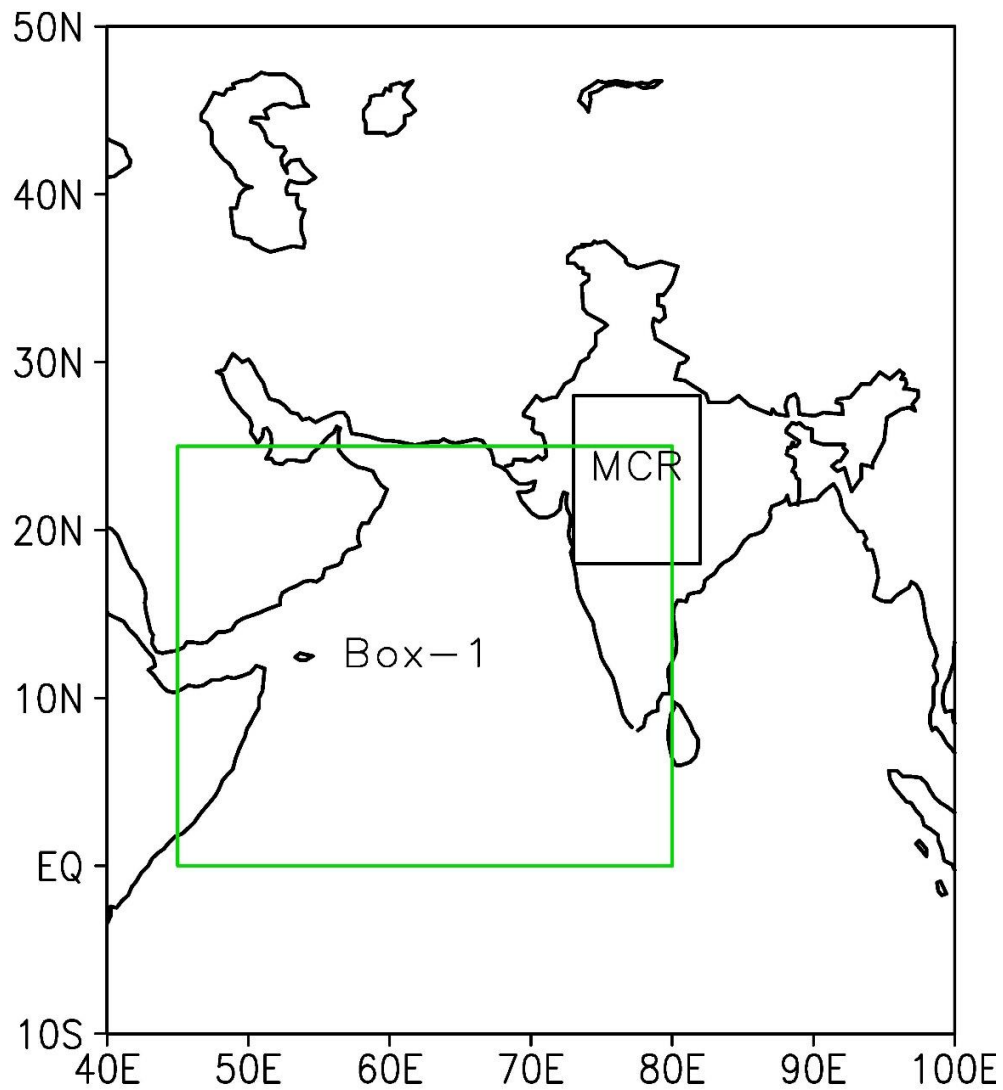
Fig.1. Study region considered over the Indian political boundary (hereafter referred to as 'India') and Indian monsoon core region (73°E-82°E and 18°N-28°N; box-MCR) along with Somali Jet PV region (45°E-80°E and 0°N-25°N; Box-1).

(a)
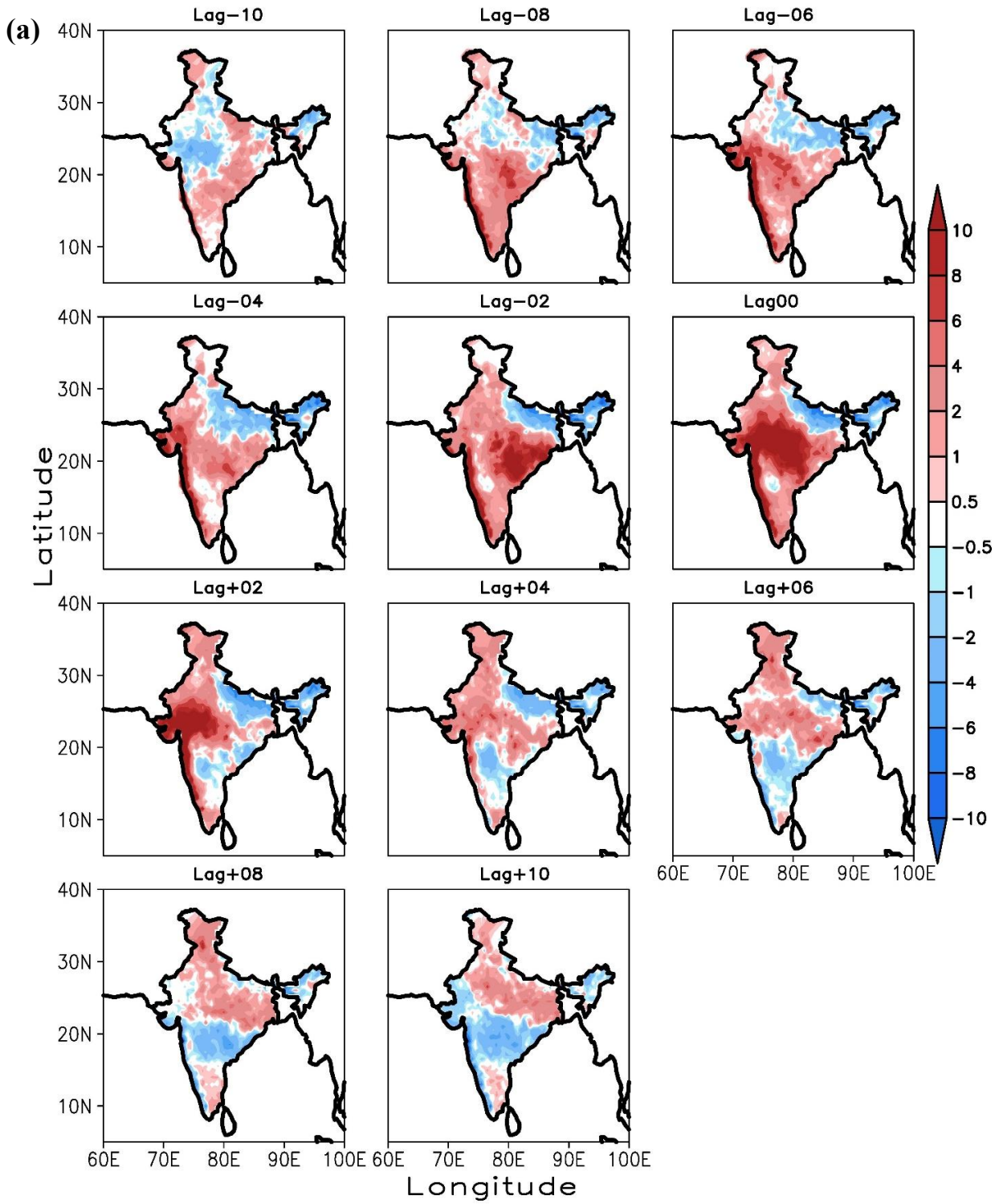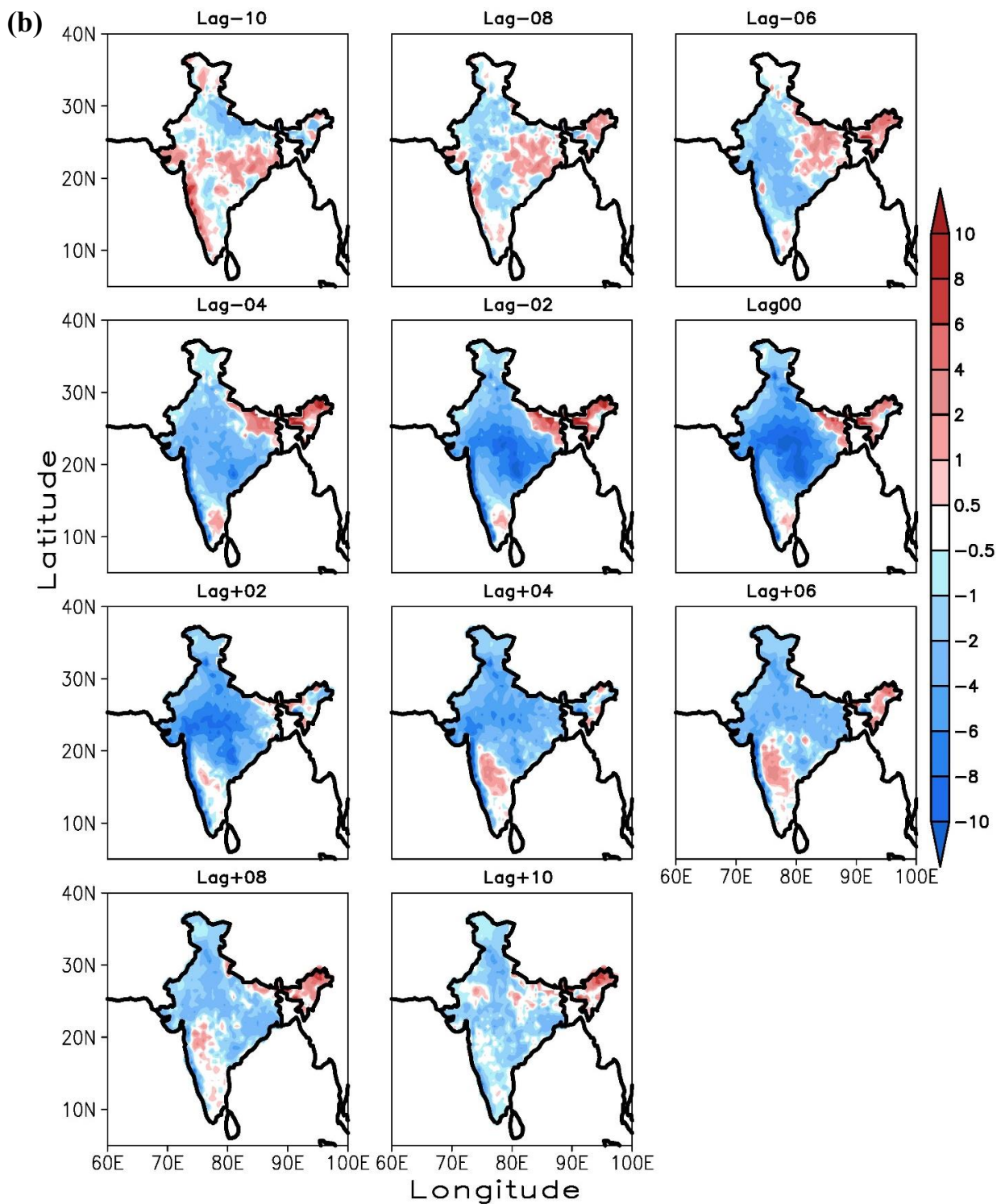
Fig. 2. Time-averaged lagged composite of daily rainfall (mm/day) anomalies from lag+10 to lag-10 for (a) active, and (b) break periods.
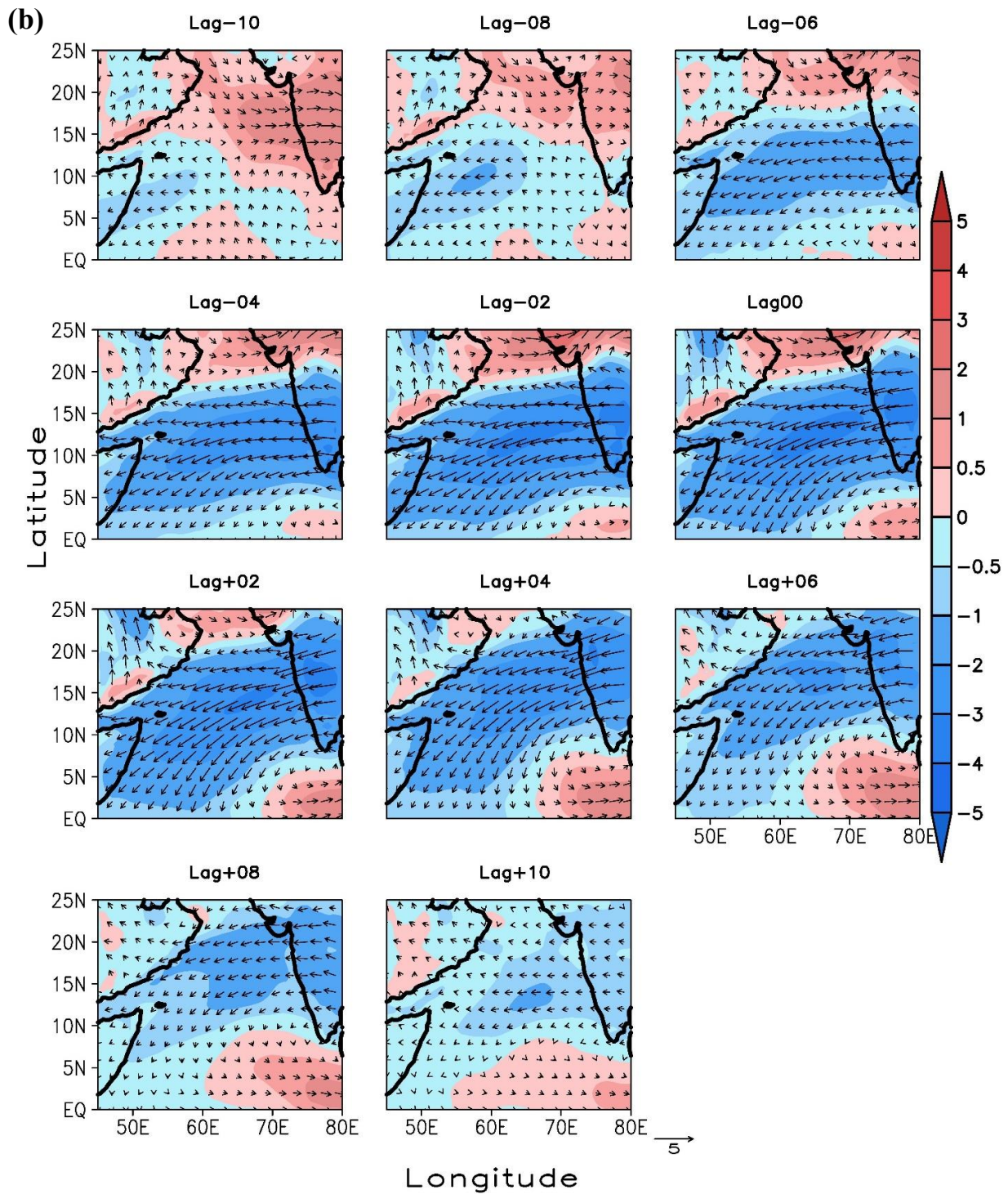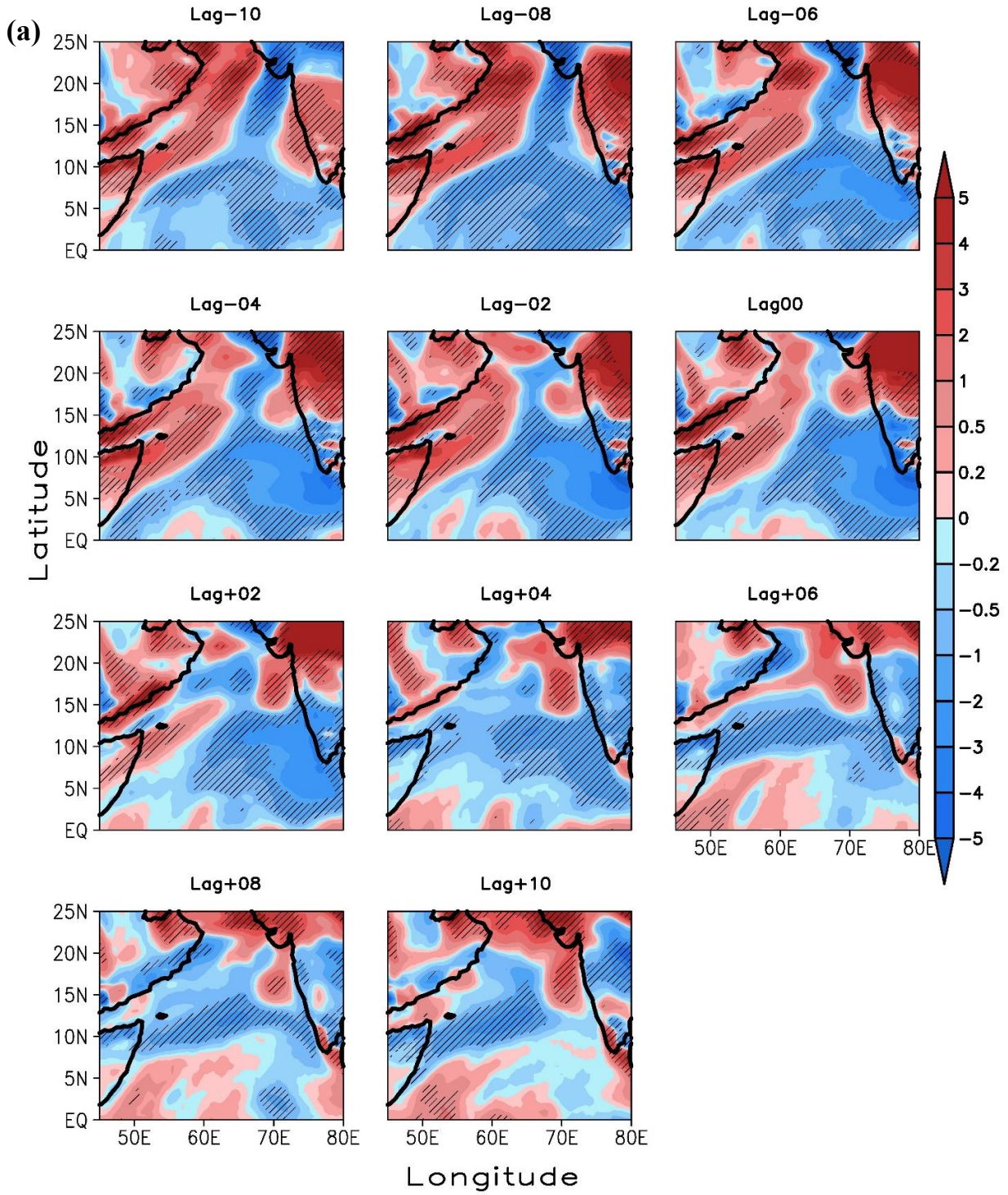
(a)
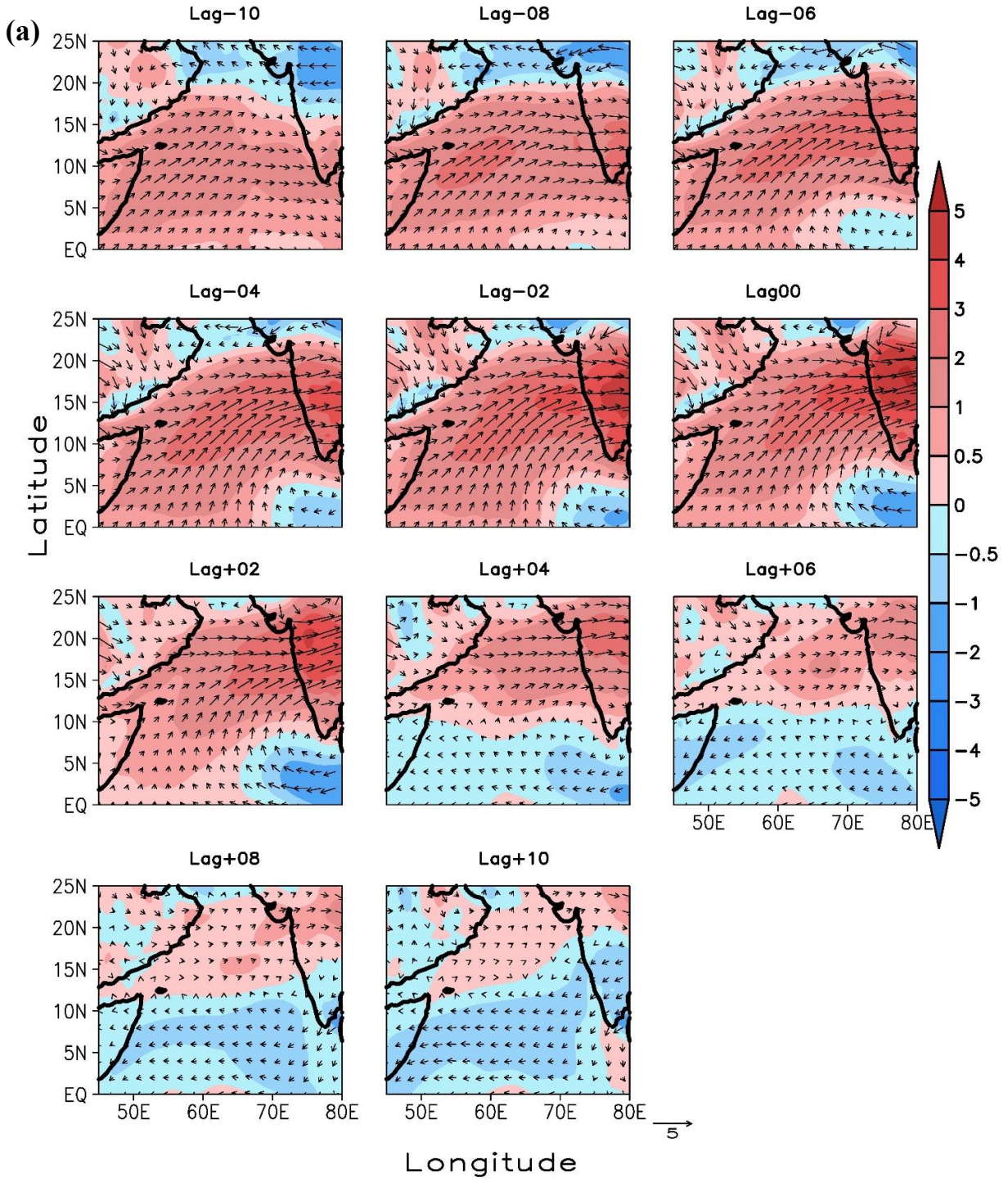
Fig. 3. Time-averaged lagged composite of daily wind anomalies at 850 hPa (magnitude; shaded, vector; 5 m/s) from -10 to +10 lag during Jul and Aug over the region 45°E-80°E and 0°N-25°N for (a) active, and (b) break periods.

(a)
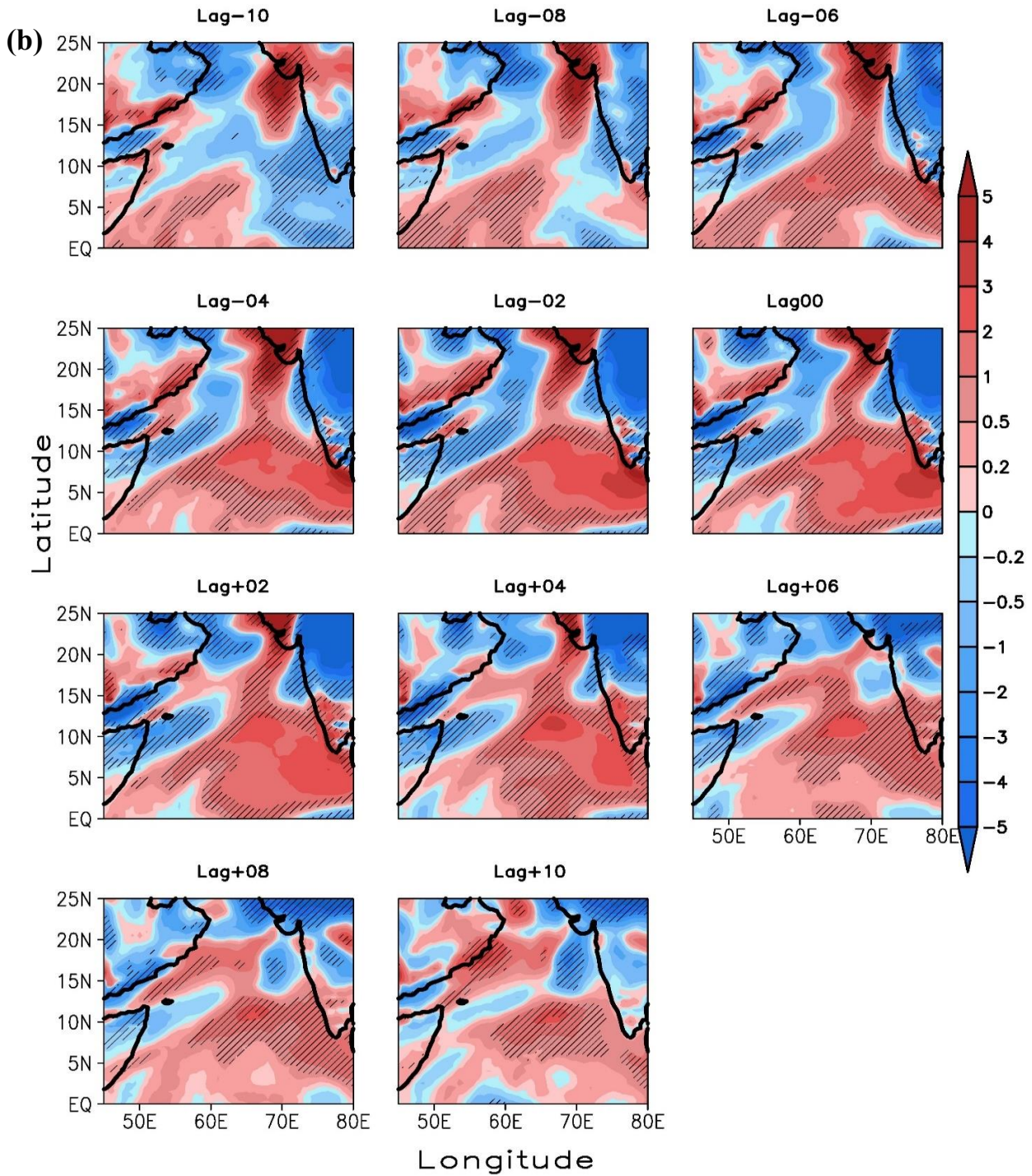
Fig. . Time-averaged lagged composite of daily Somali Jet PV (10^{-8} m^{-2} s^{-1} K kg^{-1}) anomalies at 850 hPa from -10 to +10 lag for period during Jul and Aug over the region 45°E-80°E and 0°N-25°N for (a) active, and (b) break periods. The hatched region corresponds to ≥95% significance.

(a)
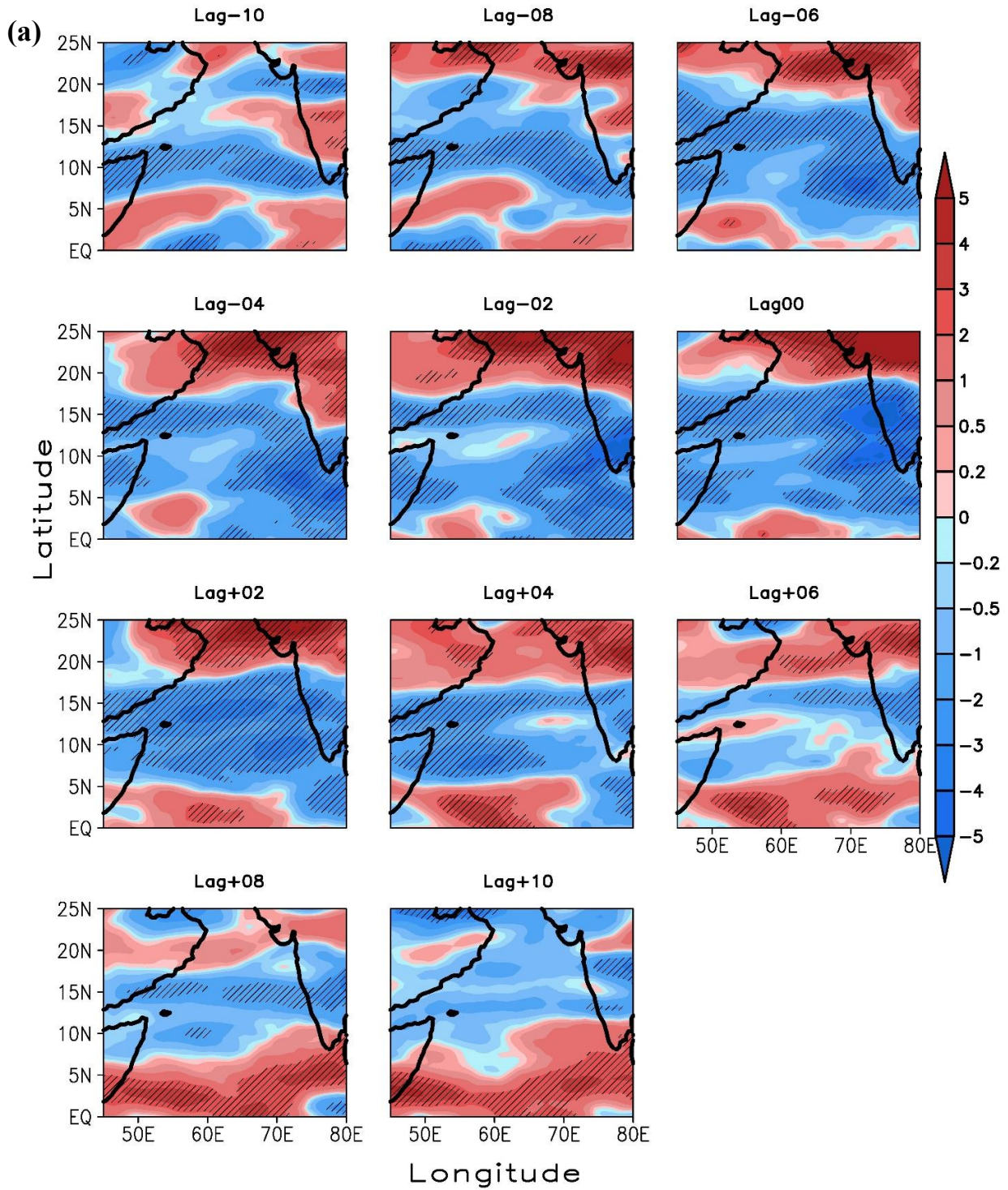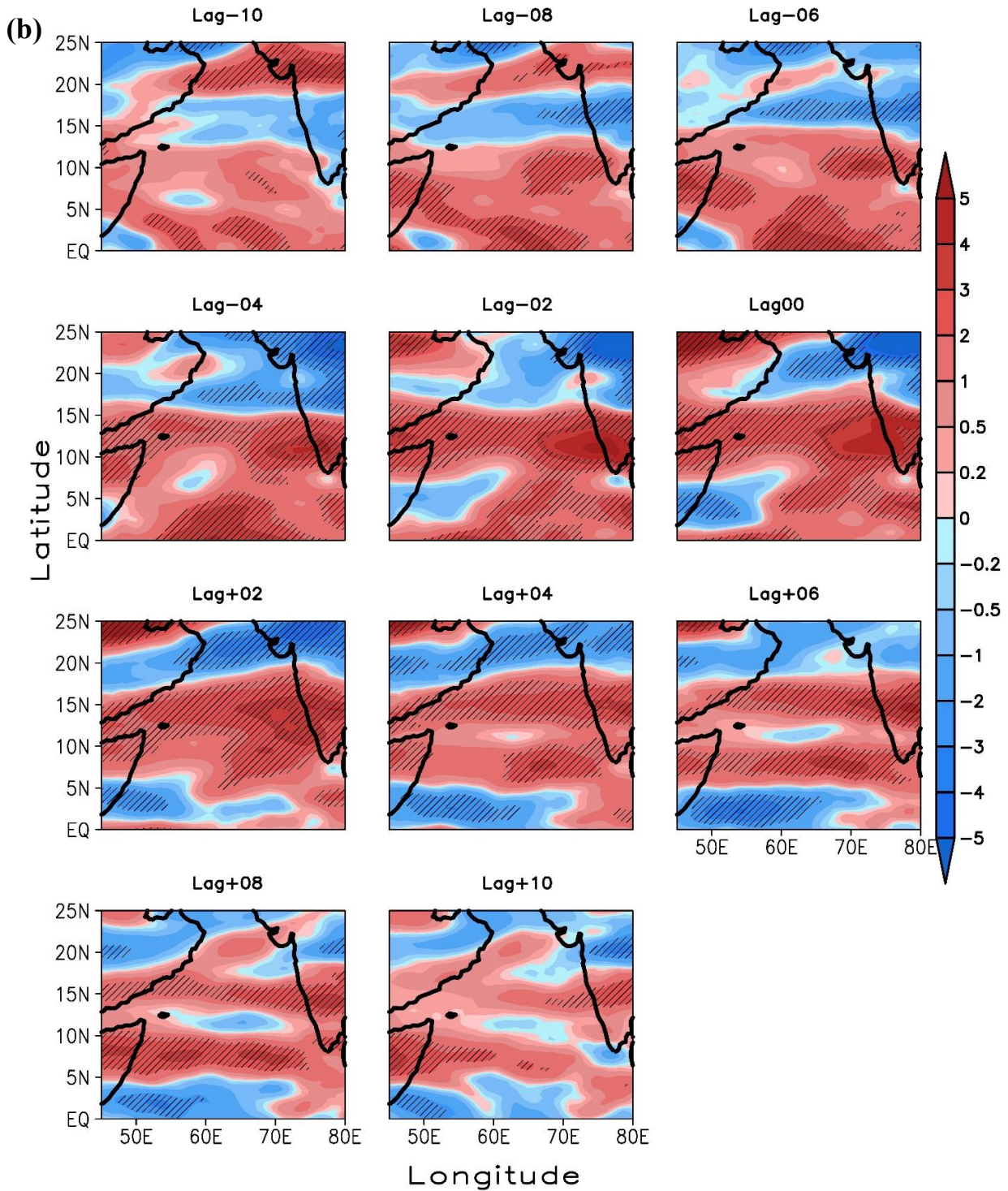
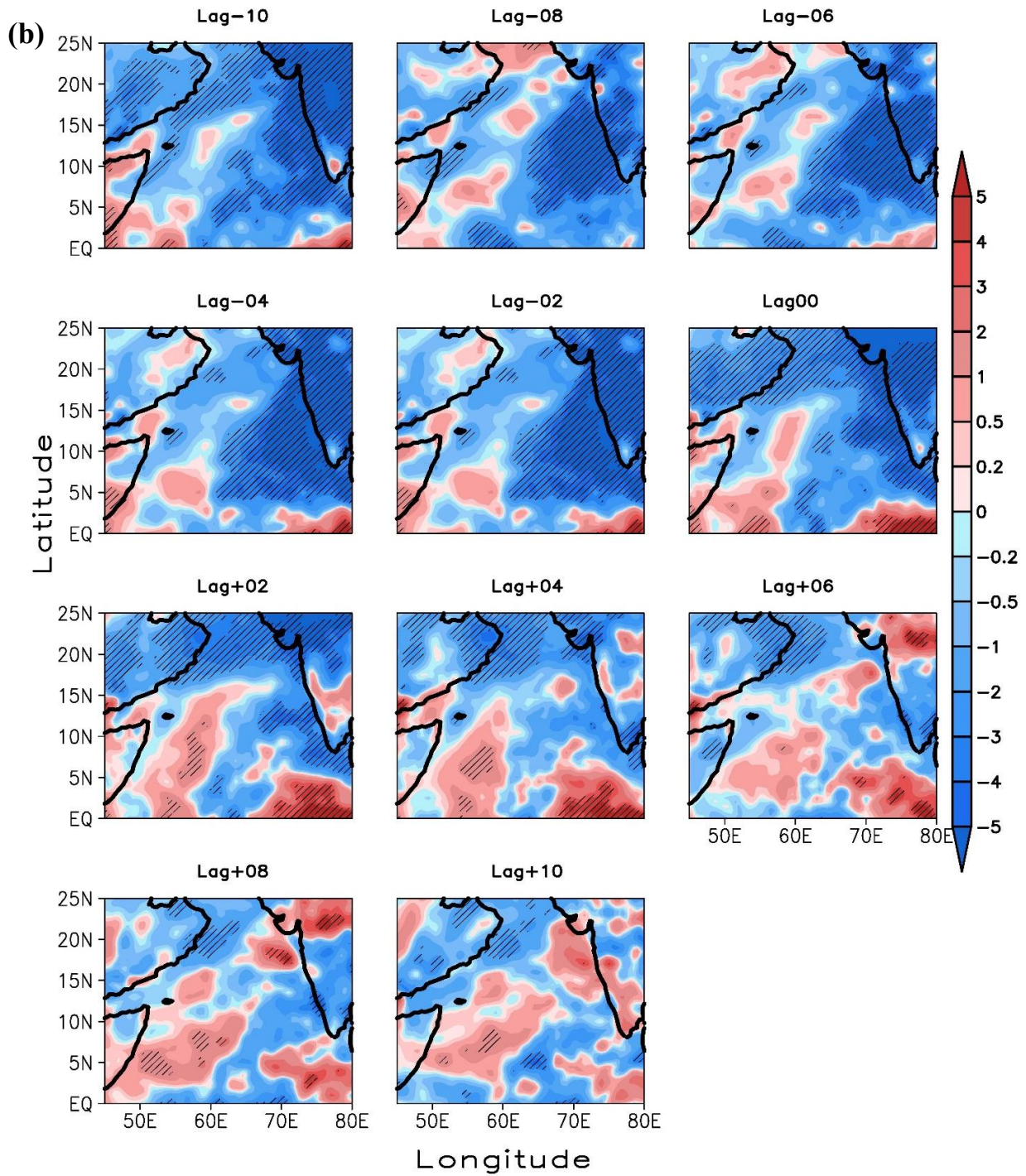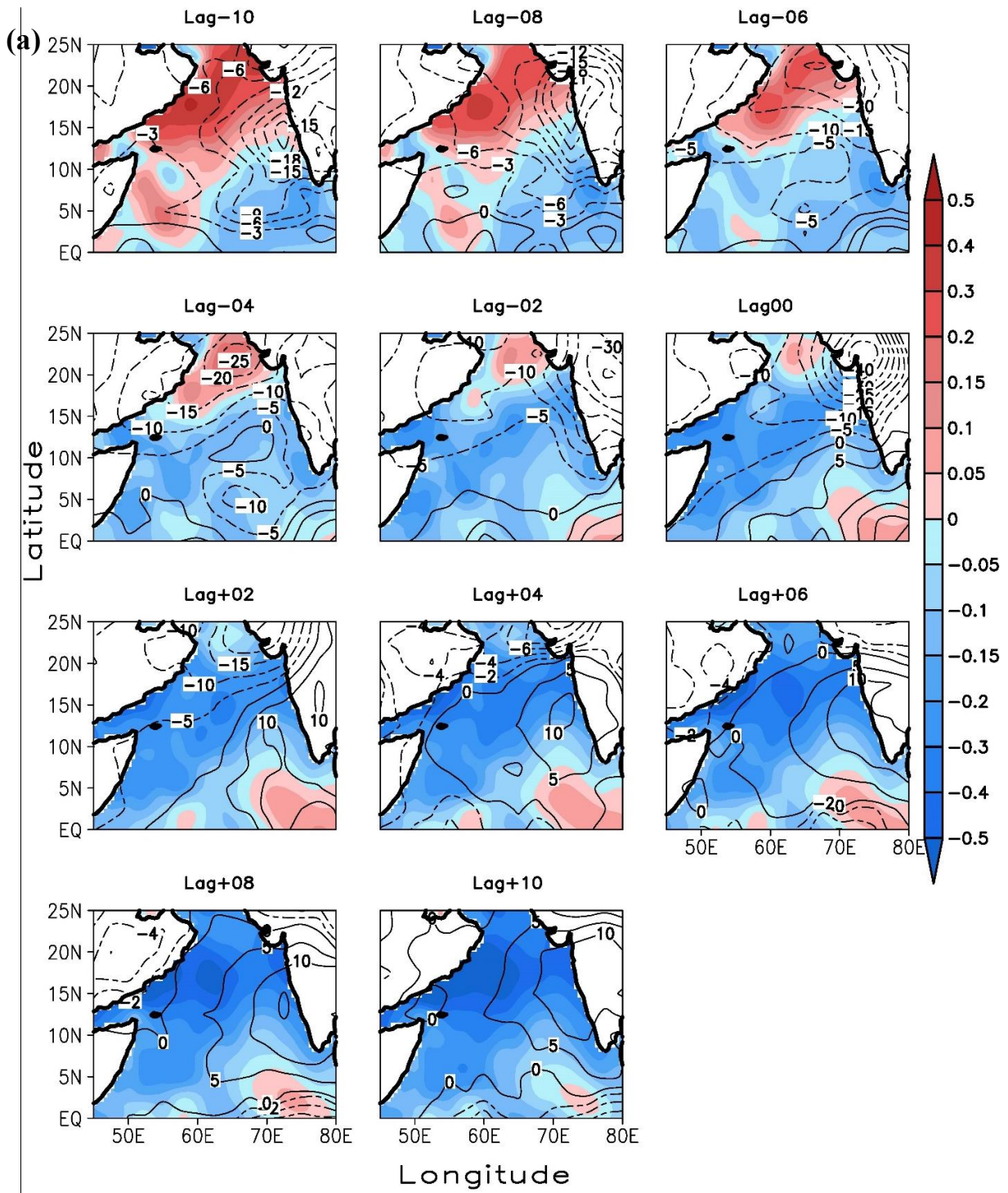Fig. 5. Time-averaged lagged composite of daily Somali Jet PV (10^{-8} m^{-2} s^{-1} K kg^{-1}) anomalies at 500 hPa from -10 to +10 lag for period during Jul and Aug over the region 45°E-80°E and 0°N-25°N for (a) active, and (b) break periods. The hatched region corresponds to ≥95% significance.

(a)
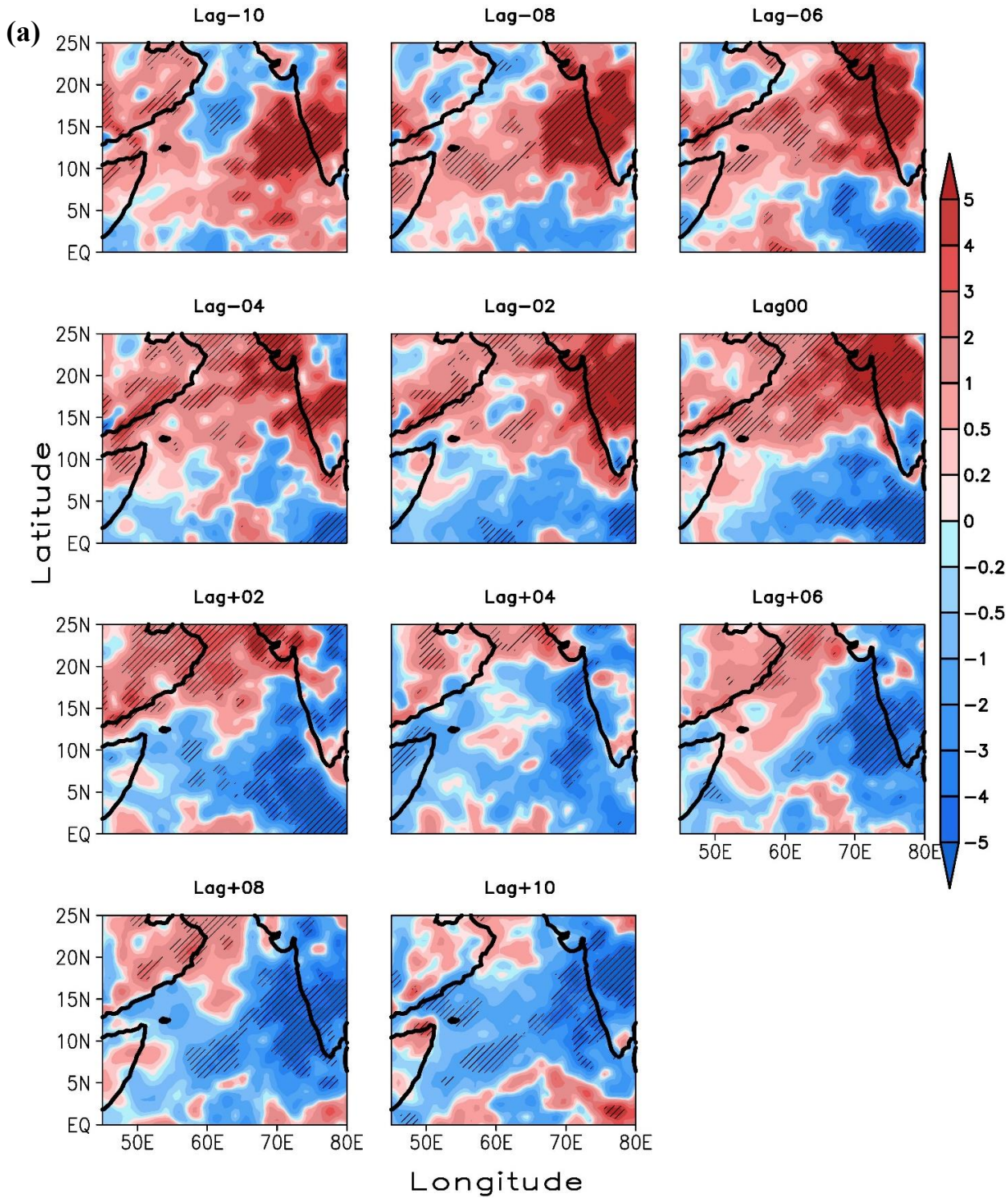
Fig 6. Time averaged lagged composite of daily diabatic heating anomalies at 850 hPa (K/day) from -10 to +10 lag for period during Jul and Aug over the region 45°E-80°E and 0°N-25°N for (a) active, and (b) break period. The hatched region corresponds to ≥95% significance.
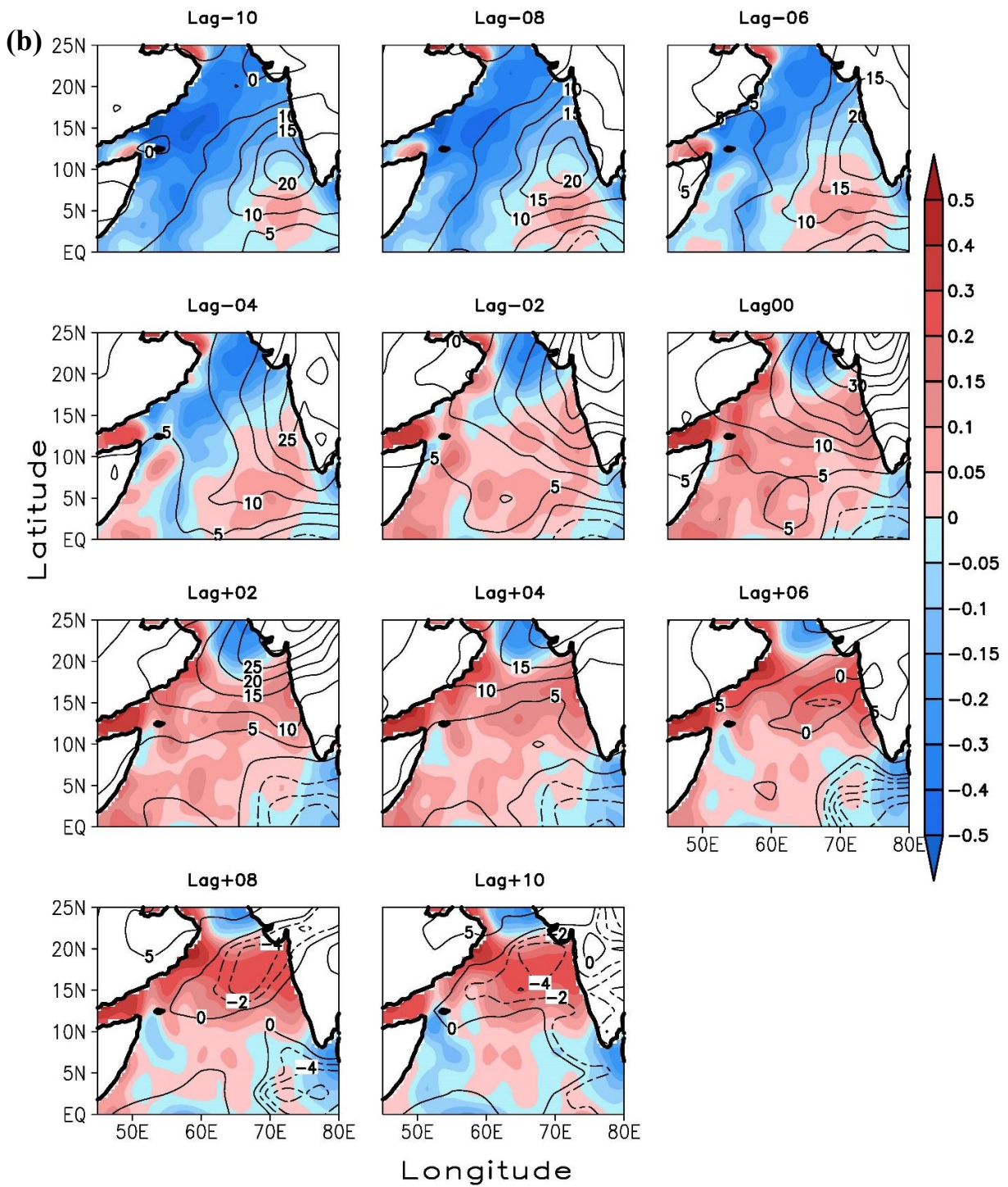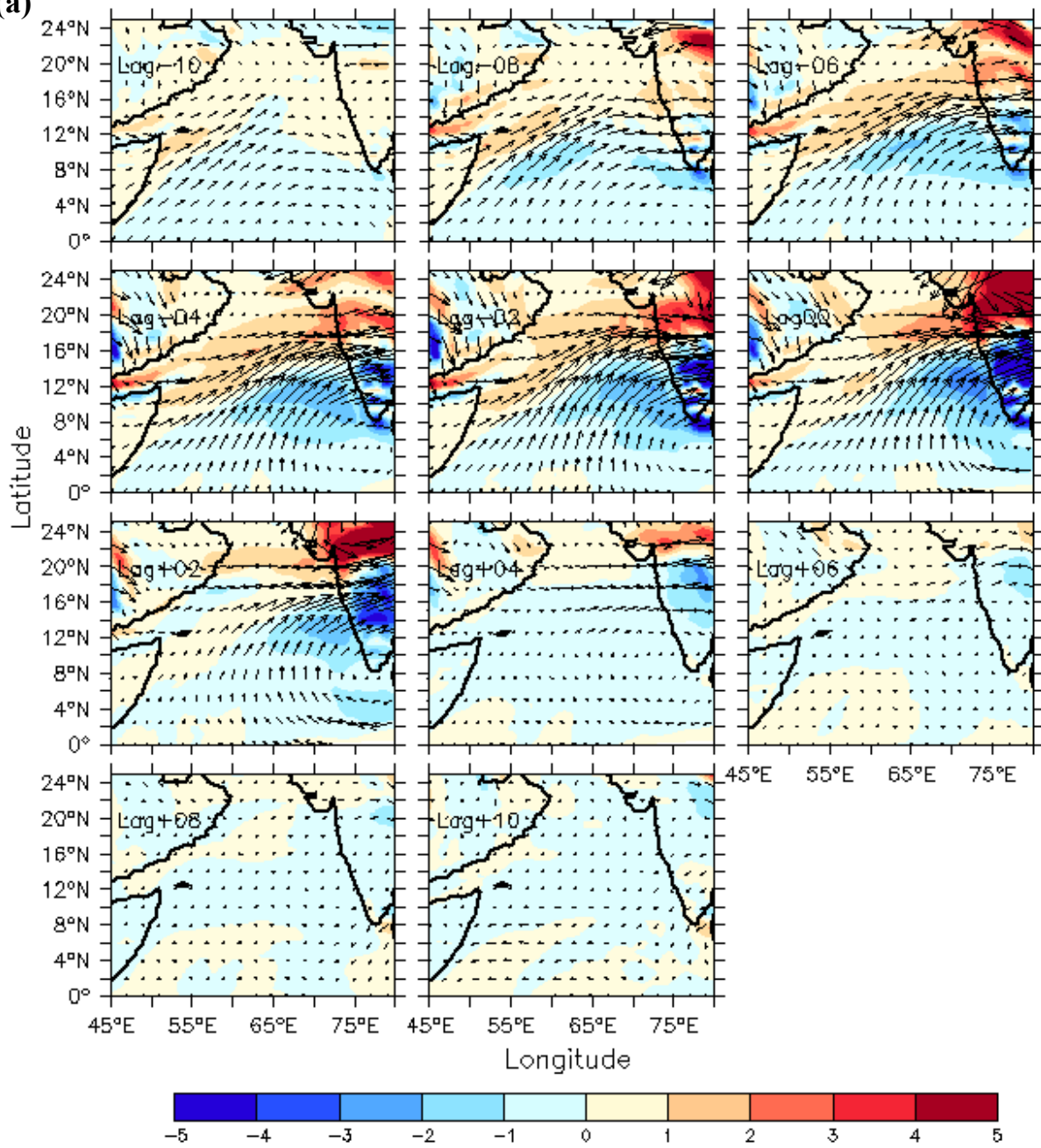
Fig. 7. Time-averaged lagged composite of daily OLR (contour) and SST (shaded) anomalies from -10 to +10 lag during Jul and Aug over the region 45°E-80°E and 0°N-25°N for (a) active, and (b) break periods.
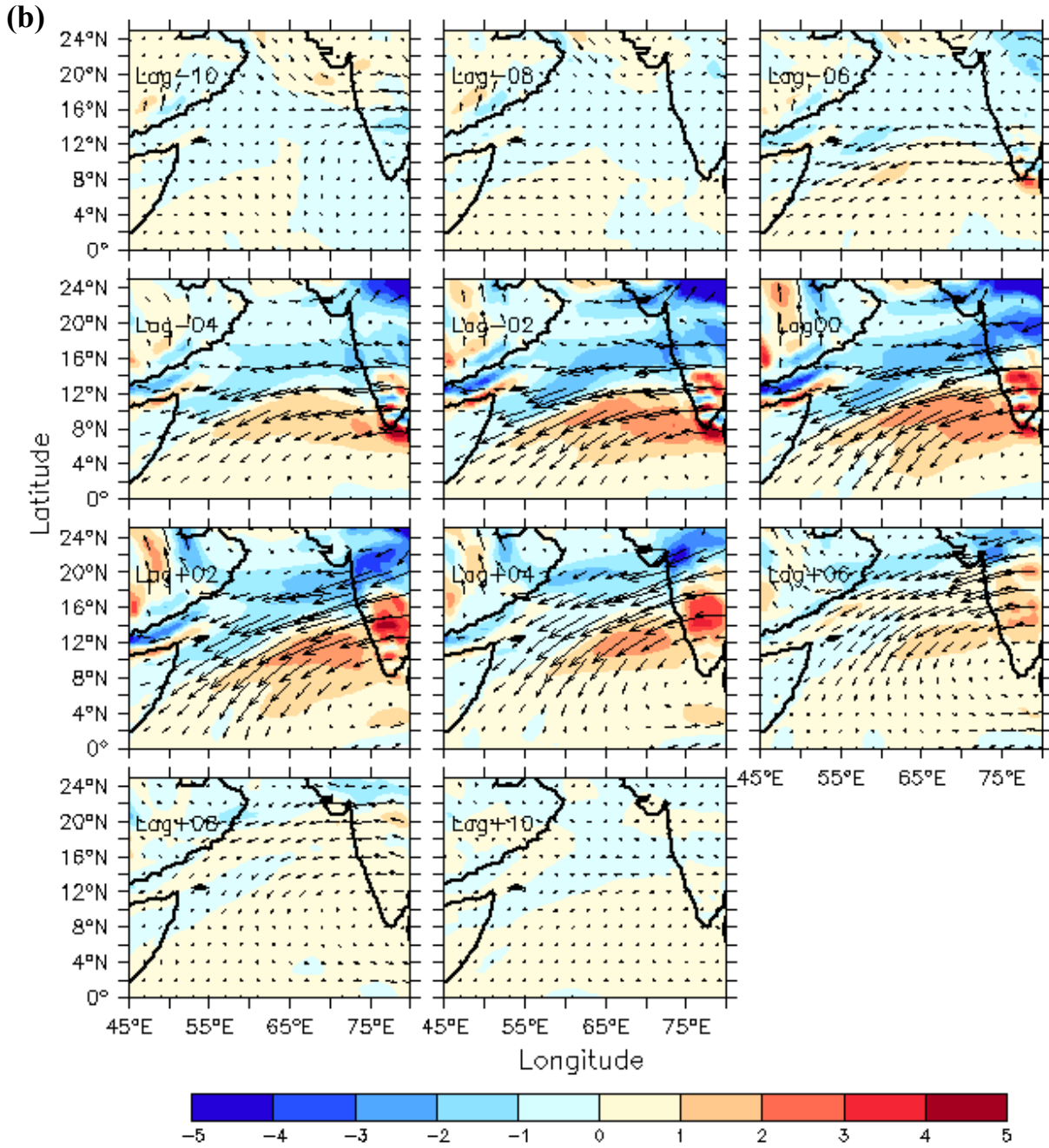
(a)

Fig. 8. Time-averaged lagged composite of wind-stress curl (shading; 1e-8 Nm^{-3}) and wind-stress (vector; Nm^{-2}) anomalies from -10 to +10 lag during Jul and Aug over the region 45°E-80°E and 0°N-25°N for (a) active, and (b) break periods.
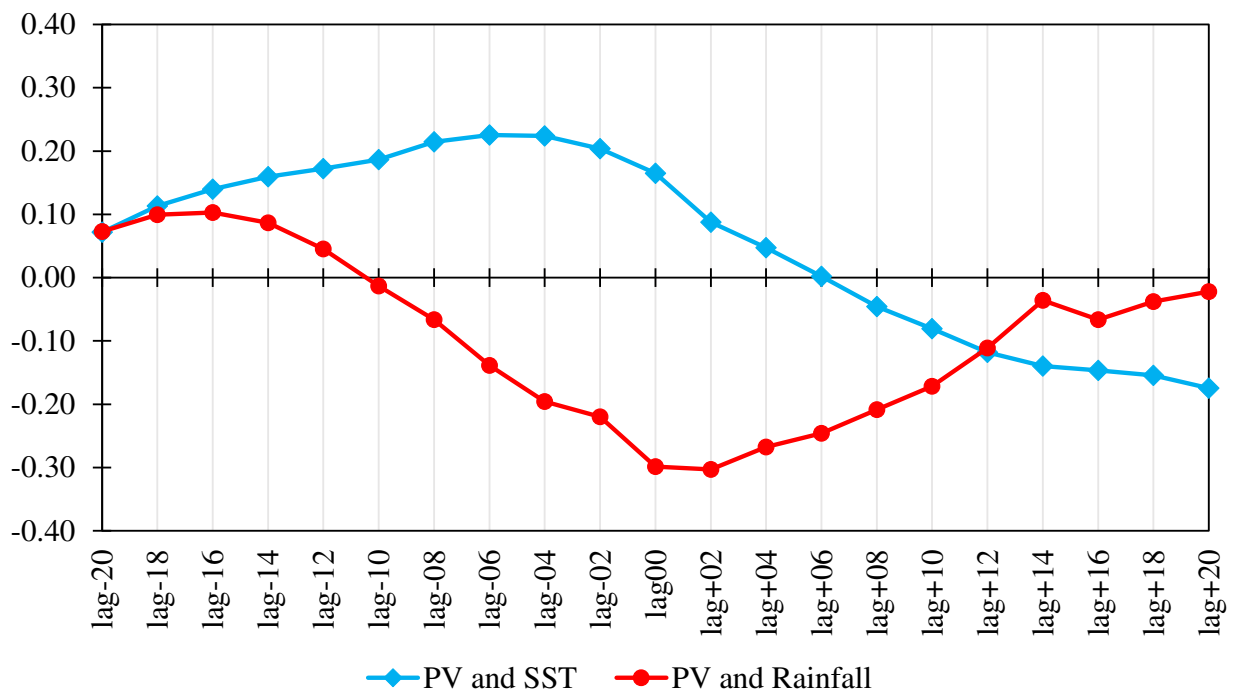
Fig. 9. Lagged correlation between area-averaged PV vs SST (SST shifting) and PV vs Rainfall (Rainfall shifting) for Jul and Aug months over the region 58°E-68°E and 6°N-12°N.
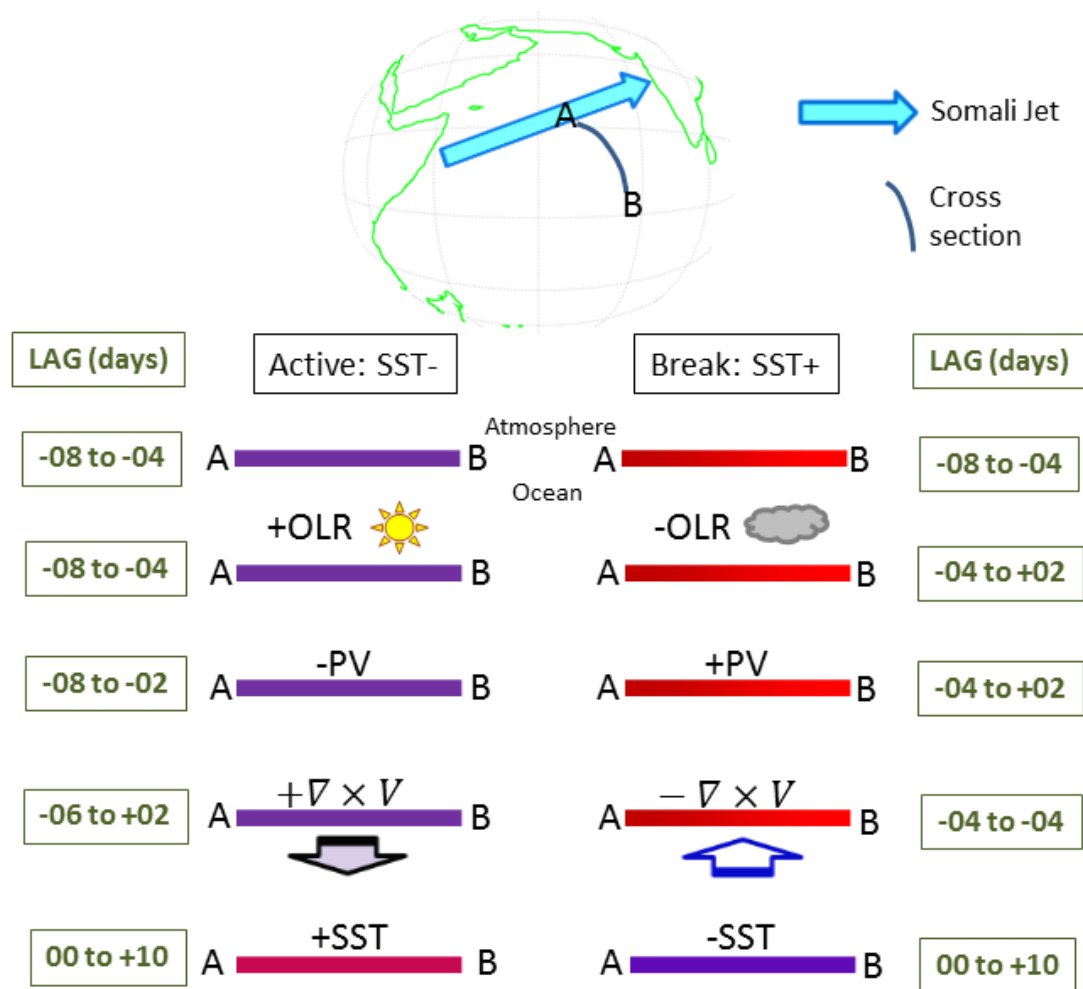
Fig. 10. Schematic showing the development of anomalies in SST, OLR, PV, wind-stress curl, upwelling and resulting SST change on the southern side of the jet in active and break phases. The lag is in days relative to the peak of active and break events as defined by rainfall over the MCR region (see text for full details).

Table 1. Active and break spells date calculated from IMD observation data at 0.5° resolution from the period 1979-2005.

Year	Active spell	Break spell
1979	3-5A, 7-10A	1-7J, 14-16A, 18-29A
1980	1-3A	-
1981	7-9J, 4-6A	24-31A
1982	21-24A	1-8J
1983	25-27J, 10-15A	7-9J
1984	2-4A, 9-11A, 16-19A	10-12J, 27-30J
1985	15-17J, 30J-1A, 7-9A	1-4J, 22-29A
1986	21-24J, 12-15A	1-6J, 23-31A
1987	24-26A	16-19J, 31J-4A
1988	25-27J	-
1989	21-24J	30J-5A
1990	22-24A	-
1991	23-25A	1-4J
1992	26-29J, 16-21A	3-10J
1993	15-17J, 3-6A	20-24J, 8-14A, 22-29A
1994	10-14J, 18-21J	-
1995	18-21J, 23-25J	2-7J, 12-16A
1996	22-28J	1-3J
1997	25-27J, 30J-2A, 22-25A	14-17A
1998	3-6J	22-26J
1999	19-21J	1-5J, 13-15A, 23-25A
2000	17-21J	23-25J, 1-8A
2001	14-16A	26-31A
2002	-	2-15J, 22-31J, 26-28A
2003	26-28J	-
2004	30J-1A, 3-6A, 9-12A	20-22J, 26-31A
2005	1-5J, 25-28J, 31J-2A	8-14A, 24-31A